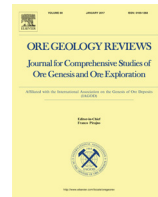




Contents lists available at ScienceDirect

Ore Geology Reviews

journal homepage: www.elsevier.com/locate/oregeo

Genesis of the Weibao banded skarn Pb-Zn deposit, Qimantagh, Xinjiang: Insights from skarn mineralogy and muscovite ^{40}Ar - ^{39}Ar dating

Jing Fang ^{a,b}, Li Zhang ^{a,*}, Huayong Chen ^{a,c}, Yi Zheng ^d, Dengfeng Li ^{a,b}, Chengming Wang ^{a,b}, Dengliang Shen ^e^a Key Laboratory of Mineralogy and Metallogeny, Guangzhou Institute of Geochemistry, Chinese Academy of Sciences, Guangzhou 510640, China^b University of Chinese Academy of Sciences, Beijing 100871, China^c Guangdong Provincial Key Laboratory of Mineral Physics and Materials, 511 Kehua Street, Guangzhou 510640, China^d Department of Earth Sciences, Sun Yat-sen University, Guangzhou 510275, China^e Geophysical and Geological Party, Xinjiang Bureau of Geology and Mineral Resource, Changji, Xinjiang 831100, China

ARTICLE INFO

Article history:

Received 8 November 2016

Received in revised form 26 May 2017

Accepted 1 June 2017

Available online xxxx

Keywords:

Weibao Pb-Zn deposit

Banded skarn

Skarn mineralogy

Muscovite ^{40}Ar - ^{39}Ar dating

Triassic metallogenesis

Qimantagh area (NW China)

ABSTRACT

The Weibao Pb-Zn deposit is located in the Qimantagh area, Xinjiang (NW China). At Weibao, stratiform Pb-Zn ore bodies are hosted by the skarn-altered Mesoproterozoic Langyashan Formation. Both of the skarn rocks and Pb-Zn ores are banded. The skarn bands are normally 0.5 to 5 cm wide and comprise alternating garnet and pyroxene zones. Systematic mineralogical studies indicate that the Weibao banded skarn was formed by infiltrative metasomatism of magmatic fluids in a disequilibrated geochemical system, rather than by the bimetasomatism between marble and Si-Al units or the metamorphism of calc-silicate-rich submarine exhalative beds. This infiltrative metasomatic process can be further divided into four stages, namely the prograde skarn, retrograde skarn, sulfide and carbonate stage. Three garnet types (Garnet I, II and III) and two pyroxene types (Pyroxene I and II) have been identified at Weibao. Garnet I has commonly Fe-rich core and Al-rich rim ($\text{Ad}_{34}\text{Gr}_{65}$ to $\text{Ad}_{96}\text{Gr}_3$), while Garnet II has a wider composition range ($\text{Ad}_{23}\text{Gr}_{73}$ to $\text{Ad}_{97}\text{Gr}_2$; average: $\text{Ad}_{59}\text{Gr}_{41}$). Garnet III is compositionally more homogeneous and Mn-rich ($\text{Ad}_{17}\text{Sp}_3\text{Gr}_{80}$ to $\text{Ad}_{55}\text{Sp}_6\text{Gr}_{35}$; average: $\text{Ad}_{47}\text{Sp}_4\text{Gr}_{49}$). Pyroxene I is diopside-rich ($\text{Hd}_{20}\text{Jd}_{79}$ to $\text{Hd}_{36}\text{Jd}_{62}$; average: $\text{Hd}_{29}\text{Jd}_{70}$), while Pyroxene II has lower diopside component ($\text{Hd}_{34}\text{Jd}_{63}$ to $\text{Hd}_{55}\text{Jd}_{13}$; average: $\text{Hd}_{48}\text{Jd}_{54}$). Garnet I and Pyroxene I may have formed by a small volume of high-temperature and volatile-rich fluids exsolved from the magmas at its initial crystallization stage. Further fractionation generated abundant magmatic fluids that reacted with the impure carbonates through infiltrative metasomatism, forming Garnet II and Pyroxene II in the banded skarn. Garnet III occurs as garnet + sphalerite + galena + calcite veinlets crosscutting the early-stage pyroxene and garnet zones, and may have been a product of late hydrothermal superimposition.

Sulfide stage is the main ore-forming stage at Weibao. Sulfide minerals in this stage precipitated mainly through replacing anhydrous (e.g., pyroxene) and hydrous (e.g., amphibole) minerals, or as interstitials among early-formed minerals. A minor amount of the sulfides also occurs as sulfide veins. The sulfide precipitation may have been controlled chiefly by physicochemical changes of ore-forming fluids and the characteristics of early-formed skarn minerals. Specifically, hydrothermal replacement of skarn minerals has provided the space for sulfide to precipitate and thus controlled their distribution, and further shaped the mineralization into a banded structure. ^{40}Ar - ^{39}Ar dating of the syn-mineralization muscovite yielded a Late Triassic age (ca. 226 Ma), which was coeval to the massive post-collisional intermediate-felsic granitoids emplacement in the Qimantagh area. Magmatic fluids evolved from these intermediate-felsic granitoids have induced the regional-scale magmatic hydrothermal mineralization, including that at Weibao.

© 2017 Elsevier B.V. All rights reserved.

1. Introduction

Skarn is well-known to host important W, Cu, Fe, Zn, Pb, Ag, Au and Sn deposits (Meinert et al., 2005). Skarn metallogenesis is a

dynamic process, and the development of a particular skarn deposit type depends on parameters such as the host rock types, geochemistry of the causative intrusions and the local tectonic history (Chen et al., 2007; Ciobanu and Cook, 2004; Meinert et al., 2005 and references therein). In this sense, one skarn deposit is commonly different from another in many aspects: In some skarn

* Corresponding author.

E-mail address: zhangli@gig.ac.cn (L. Zhang).

Cu-Zn deposits, for instance, if the magmatic fluids were relatively F-rich, Zn mineralization may occur in proximal locations rather than in typical distal locations (Chang and Meinert, 2008). At the King Island scheelite deposit (Tasmania, Australia), W-Sn-bearing skarn can be either produced by metamorphic (isochemical) process or by infiltrative metasomatism of magmatic fluids, but only that produced by the former is economic (Kwak, 2012). Skarn and the related mineralization can also occur in strike-slip shear zones which serve as fluids and heat conduit (Wan et al., 2012). Besides, some skarn Pb-Zn deposits are distinctive (from the typical calcic Pb-Zn skarn) in having stratiform orebodies and showing no visible contact between the orebodies and magmatic rocks (Liu et al., 2012; Logan, 2000; Palinkaš et al., 2013).

The Weibao deposit (Qimantagh area, NW China) is a skarn-host Pb-Zn deposit (Fig. 1). Skarn and mineralization at Weibao are featured by their banded appearance, which has given rise to the controversy of whether the Weibao Pb-Zn mineralization is modified sedimentary-type or skarn-type (Fang et al., 2015; Gao et al., 2014; Hu et al., 2010; Yang et al., 2008). The lack of apparent causative intrusions and the corresponding skarn alteration zone in/around Weibao, plus the inadequacy of age data, have further fueled this controversy. Although previous fluid inclusion and isotope studies have revealed that the Weibao ore-forming fluids were dominantly magmatic, and that the metals were contributed by both the host rocks and magmatic fluids (Fang et al., 2015), the relationships between the skarn formation (esp. its banded structure) and Pb-Zn mineralization are still ambiguous.

Considering the fact that skarn is characterized and, to some extent, defined by the occurrence of a series of calc-silicate minerals such as garnet and pyroxene, skarn minerals together with their textural characters are useful in revealing skarn forming process and conditions. For instances, 1) the overall garnet/pyroxene ratio can serve as a crude indicator of the general oxidation state of the skarn systems (Lu et al., 2003; Meinert et al., 2005); 2) geochemical changes of garnets can reveal the evolution of ore-forming fluids (Gaspar et al., 2008; Jamtveit et al., 1993; Peng et al., 2015); 3) the skarn mineral paragenesis can reveal the evolution (temperature and oxygen fugacity) pathway of the skarn system (Moecher and Chou, 1990); 4) skarn mineral textures record useful information in the primary and overprinting processes during the skarn formation (Ciobanu and Cook, 2004).

In this study, we used ore deposit geology, skarn mineralogy and their textural features to constrain the genesis of the Weibao banded skarn-host deposit. We reported the first mineralization (^{40}Ar - ^{39}Ar) age at Weibao, and propose that Weibao is a Triassic lithology-controlled skarn deposit formed in a post-collisional setting. The distinctive banded structure of the Weibao skarn may have formed by the self-organization of garnet and pyroxene during infiltration metasomatism.

2. Regional geology

Formed as the western part of the Eastern Kunlun Orogen Belt, Qimantagh area is a Paleozoic magmatic arc belt, with Qaidam basin exposed to its north, Altun Orogen to the west and Bayan Har Terrane to the south, separated by North Kunlun Fault, Southern Altun Fault and South Kunlun Fault, respectively (Fig. 1a). According to Li et al. (2008), the Qimantagh area can be further divided into three tectonic subunits from north to south with Nalingguole River Fault and Mid-Kunlun Fault as boundaries. These subunits are (I) the North Qimantagh magmatic arc; (II) the Central Kunlun massif and (III) the Early Paleozoic accretionary wedge in the South Kunlun tectonic zone (Fig. 1a).

The Qimantagh basement is composed of the Paleoproterozoic Jinshuiukou Group (detrital zircon U-Pb ages: ca. 1486–1270 Ma;

Fig. 1b; Lu et al., 2009) which consists of the Baishahe Formation (biotite plagiogneiss, migmatite, biotite-plagioclase amphibolite with marble and quartzite) and the Xiaomiao Formation (marble, gneiss, greenschist and quartzite). Other Precambrian strata include the Langyashan Formation and the Quidonggou Formation (Fig. 1b). The Langyashan Formation is mainly composed of banded marble and limestone with slate, while the Quidonggou Formation comprises silty slate and siltstone with marble. The contact relationships between these Precambrian rocks are mainly parallel unconformity. The Ordovician-Silurian Tanjianshan Group and the Baiganhu Formation are unconformably overlain on the Quidonggou Formation (Fig. 1b). The Ordovician-Silurian strata comprise marine clastic carbonates, volcanics and volcaniclastics rocks. The Devonian strata, including the Heshangou, Haerzha and Maoniushan formations, were marine-terrestrial facies sediments composed of clastics, carbonates and pyroclastic intermediate-felsic volcanics (Fig. 1b). These rocks show angular unconformity with the underlying Baiganhu Formation. Carboniferous succession mainly includes the Dagangou and Di'aosu formations, which comprise neritic clastics, biolithic carbonates and minor volcanics (Fig. 1b). Permian rocks, including the Buqingshan Group and the Gequ Formation, mainly comprise carbonates and volcanics with clastic interbeds (Fig. 1b). The Carboniferous and Permian strata are largely in conformable contact. The Triassic Elashan Formation overlies angular-unconformably on the underlying strata, and comprises continental sandy conglomerate, tuff and rhyolite (Fig. 1b).

Magmatism at Qimantagh occurred mainly in the Ordovician-Silurian and Permian-Triassic (Fig. 1b). The former contains igneous rocks ranging from ultramafics to granitoids (Fig. 1b), whilst the latter contains mainly granitoids (outcrop size: 23,000 km²) (Liu et al., 2004). The most important metallogenic event at Qimantagh occurred in the Triassic, and is space-time related to the Triassic granitoids.

Major structures at Qimantagh include NW-trending deep faults or sutures such as the North Kunlun, Middle Kunlun and South Kunlun faults. These faults controlled the intrusion emplacement and the sedimentary strata distribution, and some of them have also acted as stratigraphic boundaries (Fig. 1b).

3. Ore deposit geology

The Weibao Pb-Zn deposit is located in the North Qimantagh magmatic arc (Fig. 1). The four outcropping stratigraphic units at Weibao are the Paleoproterozoic Baishahe, Mesoproterozoic Langyashan, Permian Dachaigou and Triassic Elashan formations (Fig. 1c). Intrusive rocks at Weibao area mainly belong to Triassic granitoids (Fig. 1c). These Triassic granitoids intruded into the Langyashan Formation and yield an age of 227.6 ± 2.3 Ma (Fig. 2a; Zhou et al., 2015). NW-trending faults are widespread and are ore-controlling (Fig. 1c). The Baishahe Formation consists of marble and K-feldspar granitic gneiss (Fig. 2). The ore-hosting Langyashan Formation is composed of metamorphosed clastic and carbonate sediments (skarn, marble and schist) (Fig. 2). No intrusive rocks were found within the main oreblock of Weibao deposit (Fig. 2a).

Thirty-eight orebodies have been delineated, giving total reserves of about 1.0 Mt (Pb + Zn) and about 256 t Ag @ 1.03% Pb, 1.22% Zn and 8.53 g/t Ag (Geophysical and Geochemical Party, Xinjiang Bureau of Geology and Mineral Resource; abv. GGP). Most orebodies are banded or lenticular and stratiform (GGP; Fig. 3). Orebodies are strictly controlled by skarn alteration in the Langyashan Formation and the mineralization is distributed along fractures/joints in local folds (Figs. 3, 4a-d). The principal ore minerals are galena and sphalerite with accessory magnetite, chal-

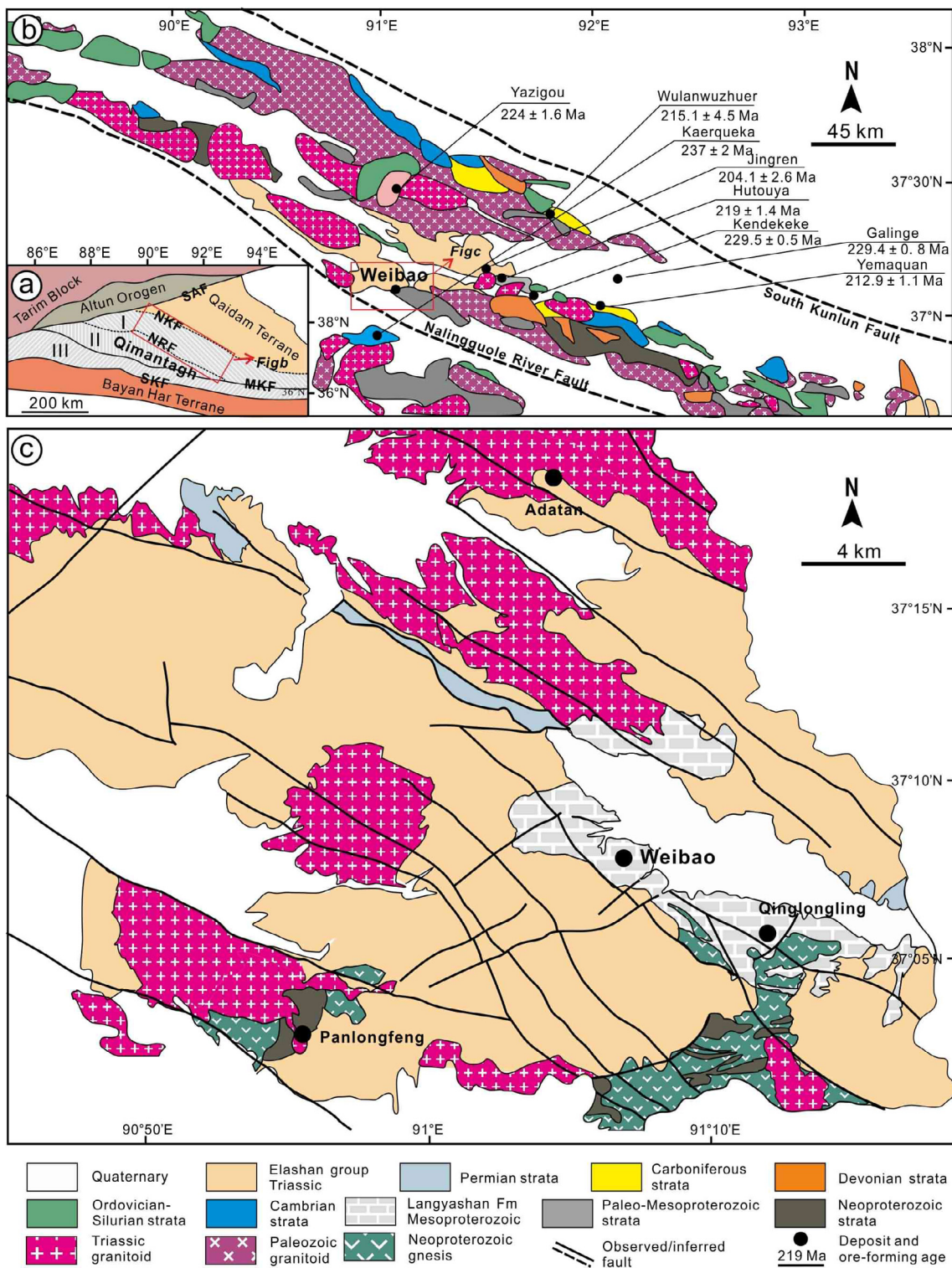


Fig. 1. Regional geological map of the Qimantagh area and the Weibao Pb-Zn district. (a) Tectonic framework of the Qimantagh area and its adjacent districts. I- the North Qimantagh magmatic arc; II- the Central Kunlun Massif; III- the Early Paleozoic accretionary wedge in South Kunlun tectonic zone. SAF- South Altun Fault; NKF- North Kunlun Fault; NRF- Nalingguole River Fault; MKF- Middle Kunlun Fault; SKF- South Kunlun Fault.

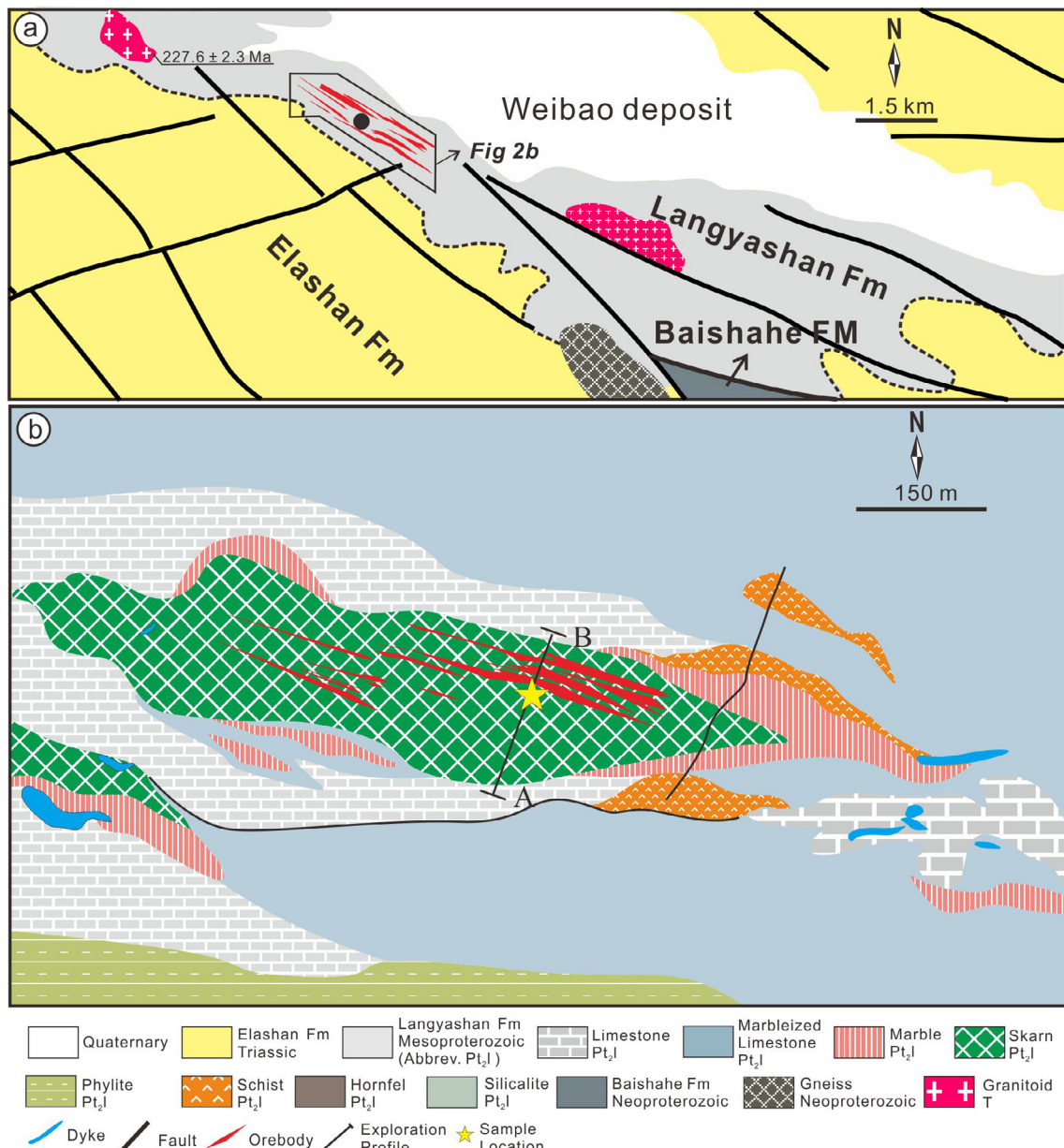


Fig. 2. (a) Geologic map of the Weibao Pb-Zn deposit. (b) Geologic map of the main ore block of the Weibao deposit, illustrating lithologic sections of the Langyashan Formation and skarn-controlled characters of ore bodies (modified after GGP, 2010). Pt₁- Paleoproterozoic; Pt₂- Mesoproterozoic; Pt₂l- Mesoproterozoic Langyashan Formation; Te- Triassic Elashan Formation.

copyrite and pyrite, whereas the gangue minerals include mainly garnet, diopside, epidote, amphibole, quartz and calcite, with minor biotite, chlorite and muscovite.

4. Skarn alteration and mineralization

4.1. Skarn alteration

The banded skarn alteration at Weibao, confined in the Langyashan Formation, is yellow to green in color (Figs. 2, 3, 4a–c). The alteration footwall is mainly composed of siliceous slate and mica schist. Unlike typical skarn deposits, the Weibao deposit shows no obvious skarn alteration zoning (Figs. 2, 3, 4a–c). The banded skarn rocks were locally faulted or folded by post-mineralization tectonic activities (Fig. 4c, d).

The Langyashan Formation (neritic-facies micritic limestone, pelite, dolomite and siltstone interbeds) was metamorphosed into marble, schist, slate and siliceous rocks (Fig. 4d, e, f). The marble normally displays calcite recrystallized texture and alternating carbonate-argillaceous banded structure (Fig. 4e, f).

The banded skarn (0.5 to 5 cm wide) is yellowish-green or gray, and the skarn minerals are commonly too fine to be identified with naked eyes (Fig. 5a, b). The banded skarn contains alternating garnet and pyroxene zones (Fig. 5). Based on the skarn mineral assemblage, morphology and paragenetic relationships, the Weibao banded skarn rocks exhibit three patterns. Pattern I: Subhedral pyroxene aggregates distributed along the straight boundaries of the pelitic layer, constituting the outer part of the skarn bands; and the complexly zoned, subhedral-anhedral garnet zone located in the inner part (Fig. 5a, c–e). Locally, Pattern I skarn band is almost totally composed of garnet, with only very thin pyroxene

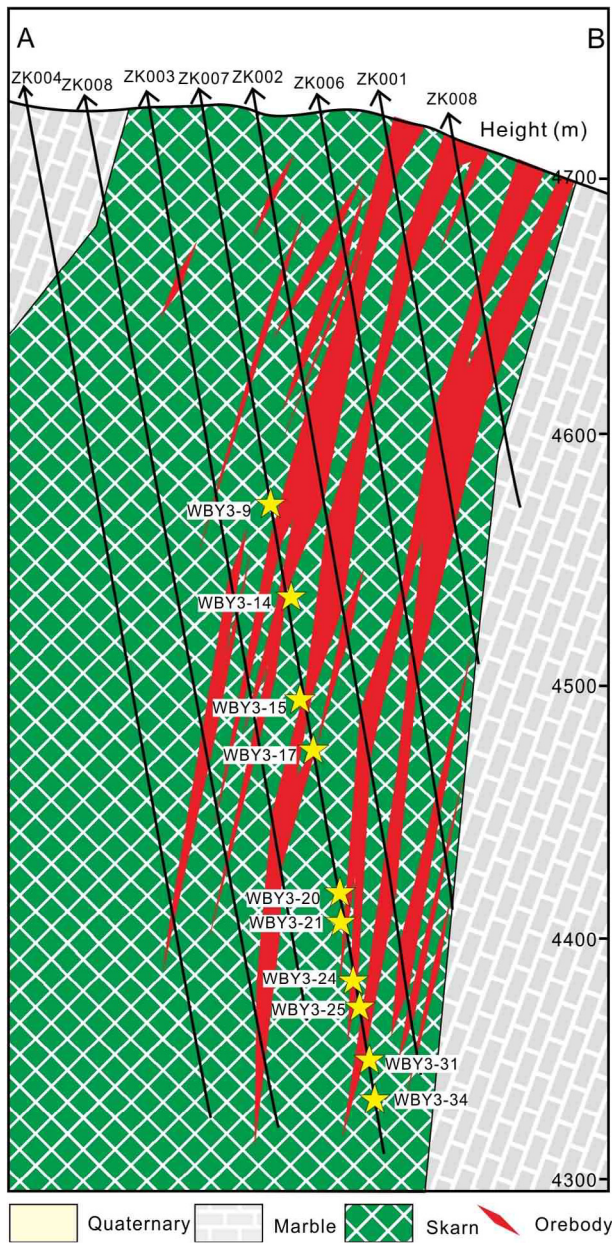


Fig. 3. No. 0 Exploration Profile of the Weibao deposit, showing the sampling locations (modified after GGP, 2010).

zone on both sides of the garnet layer (Fig. 5c). Epitaxial pyroxene veins from the pyroxene zone commonly occur and crosscut the pelite layer in the Pattern I skarn bands (Fig. 5d). Garnet in the bands is frequently replaced and crosscut by retrograde alteration minerals or late veins (Fig. 5a, e). Pattern II: Banded skarn is totally composed of pyroxene with no garnet (Fig. 5f). Pyroxene in Pattern II skarn bands is extensively altered into anhedral epidote, mica and sulfides (Fig. 5g). Pattern III skarn bands are generally fine (<1 cm wide) (Fig. 5h). Pyroxene and garnet are euhedral-subhedral and show equilibrium boundaries with the residual carbonate matrix (Fig. 5h). Garnet in Pattern III skarn bands is finer than that in Pattern I skarn bands (Fig. 5h). Generally, the Weibao skarn occurrence is dominated by Pattern I and II, with minor Pattern III.

The Weibao skarn alteration and mineralization processes can be divided into four stages *i.e.*, the prograde skarn, retrograde skarn, sulfide and carbonate stage (Fig. 6). The prograde skarn

stage is characterized by the formation of anhydrous minerals, *e.g.*, garnet and pyroxene, which occur mainly in the banded skarn and minor in marble (Figs. 5, 6, 7a–h). Mineral assemblage of retrograde skarn stage mainly consists of epidote, amphibole, biotite, quartz, calcite and minor sericite (Figs. 5e–h, 6, 7d–j). As the main mineralization stage, the sulfide stage contains mainly galena and sphalerite with minor chalcopyrite and pyrite (Figs. 5e, g, h, 6, 7g, h, j, 8). Gangue minerals in the sulfide stage include muscovite, chlorite, quartz and minor epidote and calcite. The carbonate stage is mainly represented by calcite ± quartz ± chlorite veins that crosscut the banded skarn (Fig. 7k, l).

4.2. Mineralization

Mineralization at Weibao is mainly host by banded skarn rocks and genetically related with the skarn alteration. In most cases, mineralization occurs as anhedral galena and sphalerite altering pyroxene and garnet aggregates in the skarn bands (Figs. 5a, b, g, 7g, h). Sulfides coexist with quartz locally to form massive ores (Fig. 8b). In some places, galena and sphalerite occur as veins cross-cutting the banded skarn (Figs. 5e, 7e). In Pattern III skarn bands, galena and sphalerite are subhedral and coarser, and occur as monocrystals replacing residual carbonate matrix (Fig. 5h).

5. Skarn mineralogy

5.1. Sampling and methodology

The investigated samples were collected from the drill core ZK007 of No. 0 Prospecting Line at Weibao (Fig. 3), with the detailed sample description given in Appendix A. Geochemical analysis of skarn minerals was performed with an EPMA-1600 electron microprobe at the Key Laboratory of Mineralogy and Metallogenesis of Guangzhou Institute of Geochemistry, Chinese Academy of Sciences (GIGCAS). The operating conditions consisted of an acceleration voltage of 15 kV, a beam current of 18 nA and a beam diameter of 1 μm. Vanadium concentrations were corrected by analyzing V-free and Ti-bearing standards of rutile and native Ti, because of the overlapping Ti Kβ and V Kα peaks (Carmichael, 1966). The precisions of major and trace elements were better than 2% and 5%, respectively. Matrix corrections were performed by the ZAF procedures (Jurek and Hulínský, 1980).

5.2. Garnet

Garnet at Weibao commonly occurs in banded skarn, marble, or as garnet + sphalerite + galena + calcite veinlets crosscutting the skarn band (Figs. 5, 7a–e). Three types of garnets have been distinguished, *i.e.*, Garnet I, II and III. Garnet I generally occurs as speckled monocrystals or aggregates in the marble (Figs. 7a–c, 9a). These garnet grains are euhedral, medium-grained, orange to brown in color, and generally exhibit anisotropy, oscillatory zoning or polysynthetic twining (Figs. 7c, 9a). Garnet II is hosted by the banded skarn and forms the inner part of skarn band with pyroxene zones on its both sides (Fig. 5). Garnet II grains are mostly subhedral to anhedral, medium-coarse-grained, reddish in color, and show anisotropy but without twinning (Figs. 5, 7d, 9b). Different to Garnet I which has isolated distribution and lower crystal birefringence (Figs. 7b, c, 9a), Garnet II generally occurs as banded aggregates and show chaotic birefringence (Figs. 5, 7d, 9b). Commonly, Garnet II is extensively fractured and replaced by later minerals or crosscut by veins (Figs. 5, 7d, e). Garnet III occurs as garnet + sphalerite + galena + calcite veinlets crosscutting the banded skarn (Fig. 7e). These garnet grains are subhedral to anhedral, and are distributed along the veinlet walls in a comb-like

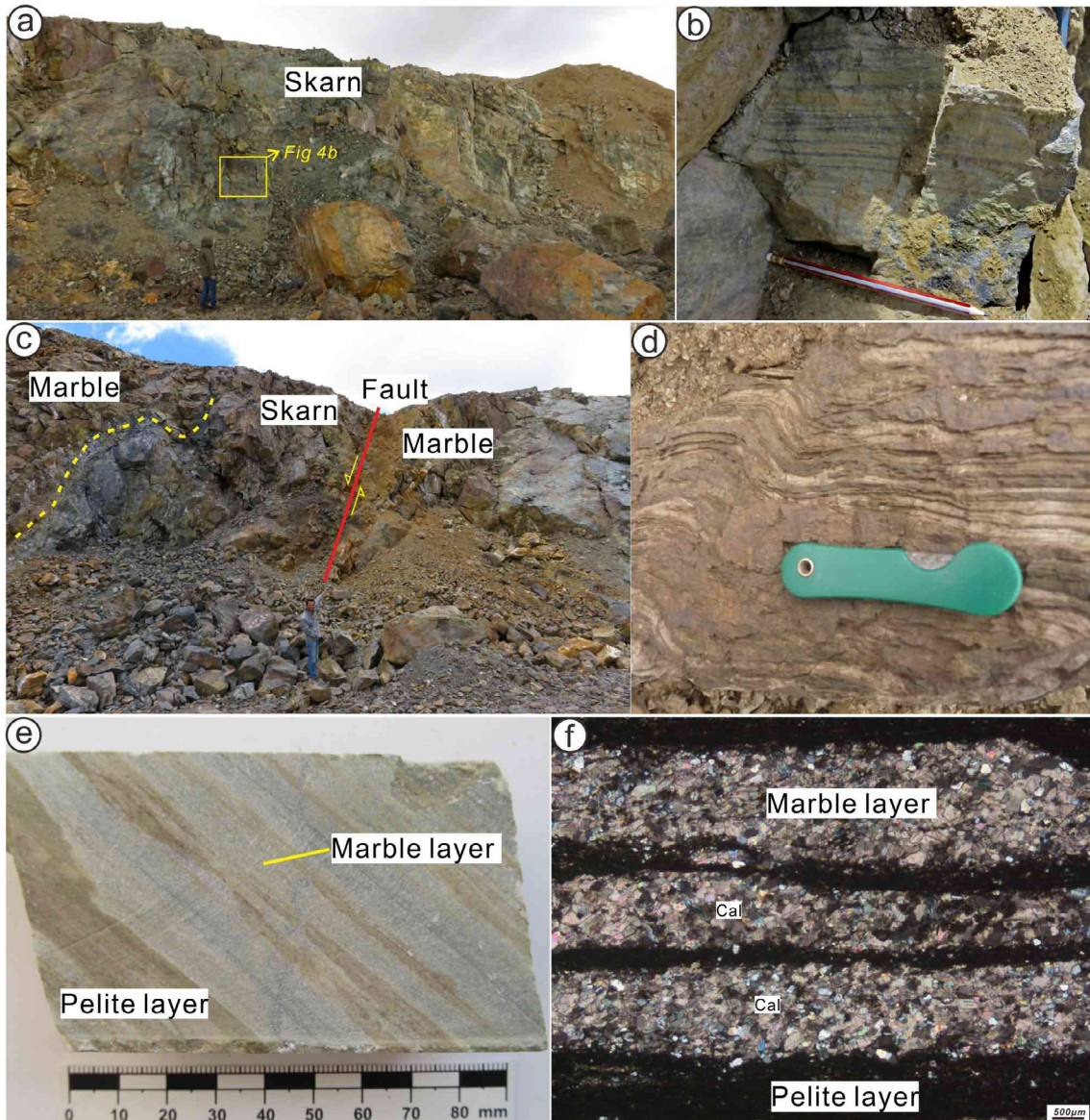


Fig. 4. (a) Skarn outcrop at Weibao, with details shown in b. (b) Banded skarn and mineralization. (c) Contact between skarn and marble. (d) Banded limestone with its interbedded pelitic protolith. (e) Marble with its interbedded pelitic protolith. (f) Photomicrograph of marble, showing the marble-pelite interbedded structure.

structure (Fig. 7e). Garnet III is normally isotropic and has typical dissolution texture. The Weibao garnet population is dominated by Garnet II (~90%). Garnet I and II belong to the prograde skarn stage (Fig. 6), while Garnet III may have formed by later hydrothermal superimposition.

All the three garnet types belong to the grossular-andradite solid solution series ($\text{Ad}_{17}\text{Gr}_{81}$ to $\text{Ad}_{96}\text{Gr}_1$) (Table 1; Fig. 10a). Garnet I normally has an Fe-rich core and Al-rich rim with limited compositional zoning (Table 1; Figs. 9a, 10a). Locally, some fine garnet grains are homogeneous in composition and Al-rich (Table 1; Figs. 9a, 10a). Garnet II is compositionally heterogeneous ($\text{Ad}_{23}\text{Gr}_{73}$ to $\text{Ad}_{97}\text{Gr}_2$; average $\text{Ad}_{59}\text{Gr}_{41}$) (Table 1; Figs. 9b, 10a), whereas Garnet III is more homogeneous ($\text{Ad}_{17}\text{Sp}_3\text{Gr}_{80}$ to $\text{Ad}_{55}\text{Sp}_6\text{Gr}_{39}$; average $\text{Ad}_{47}\text{Sp}_4\text{Gr}_{49}$) and Mn-rich (Table 1; Fig. 10a).

5.3. Pyroxene

Pyroxene is the most abundant skarn mineral at Weibao, and can be divided into two types (both belong to the prograde skarn

stage). Pyroxene I occurs in the skarnized marble as sparse disseminations or aggregates (Figs. 7a, b, f, 9c). These pyroxene grains are generally euhedral, coarse-grained and coexist with Garnet I (Figs. 7a, b, f, 9c). Pyroxene II occurs in banded skarn as aggregates (Figs. 5, 7g, h, 9d). These pyroxene grains coexist with Garnet II and were partly replaced by retrograde alteration minerals or crosscut by later veins (Figs. 5, 7g, h).

EMPA results show that the Weibao pyroxene belongs to the diopside-hedenbergite-johannsenite solid solution series. Pyroxene I is diopside-rich ($\text{Hd}_{20}\text{Jo}_1\text{Di}_{79}$ to $\text{Hd}_{36}\text{Jo}_2\text{Di}_{62}$; average $\text{Hd}_{29}\text{Jo}_1\text{Di}_{70}$) (Table 2; Figs. 9c, 10b), whereas Pyroxene II has lower diopside content ($\text{Hd}_{34}\text{Jo}_3\text{Di}_{63}$ to $\text{Hd}_{55}\text{Jo}_{13}\text{Di}_{32}$; average $\text{Hd}_{48}\text{Jo}_5\text{Di}_{47}$) (Table 2; Figs. 9d, 10b).

5.4. Epidote

Euhedral to subhedral epidote is the most abundant retrograde alteration minerals, and occurs as (1) disseminations in marble associated with Garnet I (Fig. 7a, b); (2) fine-grained crystals or

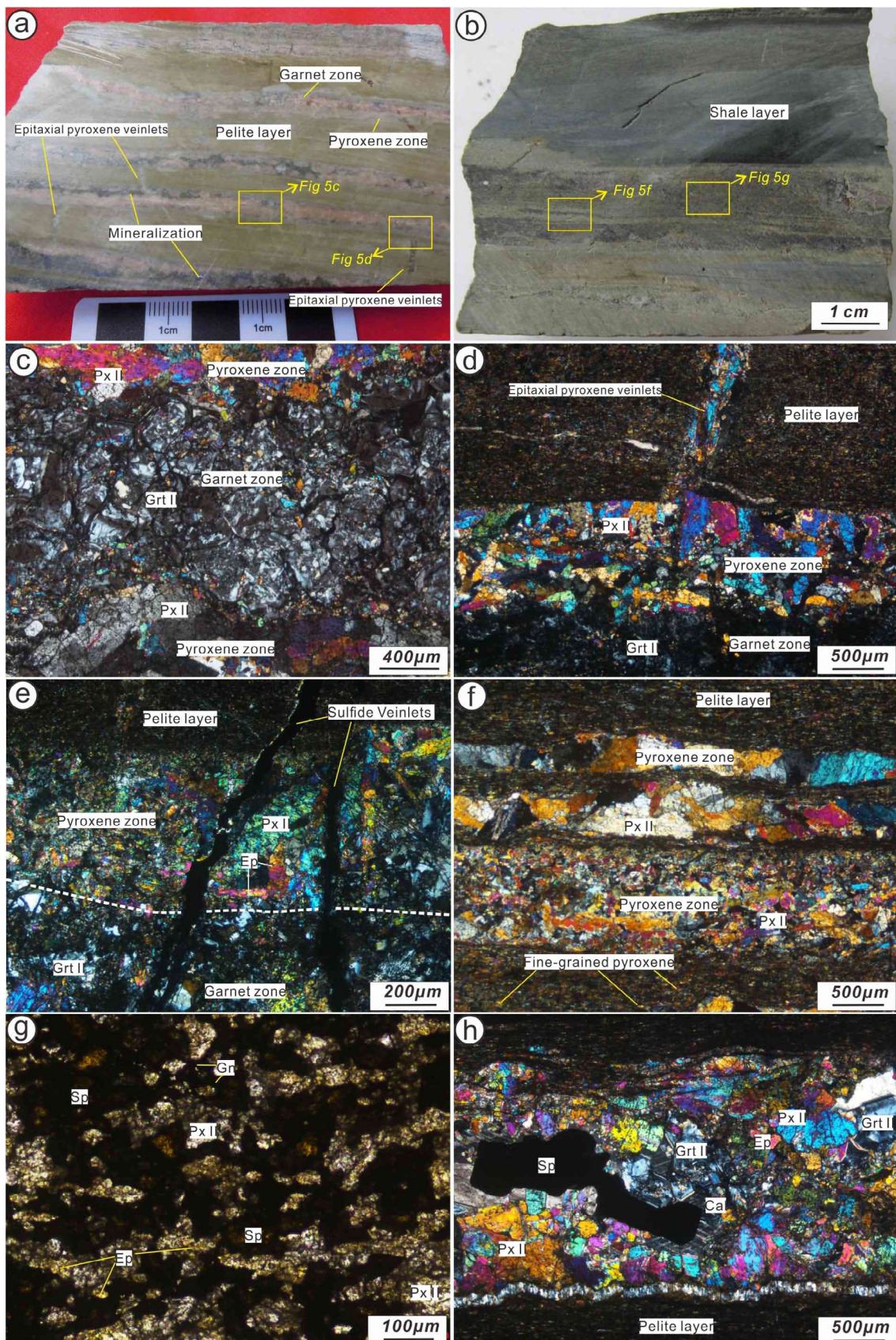


Fig. 5. Photos of banded skarn and mineralization of the Weibao deposit. (a)–(b) Drill core sample showing typical banded skarn and mineralization, with details shown in c–g. (c) Alternating garnet and pyroxene zones. (d) Interlayered garnet zone and pyroxene zone in the banded skarn with epaxial pyroxene veinlets cutting through the pelitic layer. (e) Sulfide veins crosscut garnet, pyroxene zone and pelitic layer. (f) Banded skarn (layered pyroxene) zone. (g) Epidote, sphalerite and galena replaced fine-grained pyroxene aggregates in banded skarn, shaping mineralization into a banded structure. (h) Euhedral sphalerite replaced residual calcite in the interstices of garnet and pyroxene. Abbr: Grt, garnet; Px, pyroxene; Ep, epidote; Qz, quartz; Gn, galena, Sp, sphalerite; Cal, calcite.

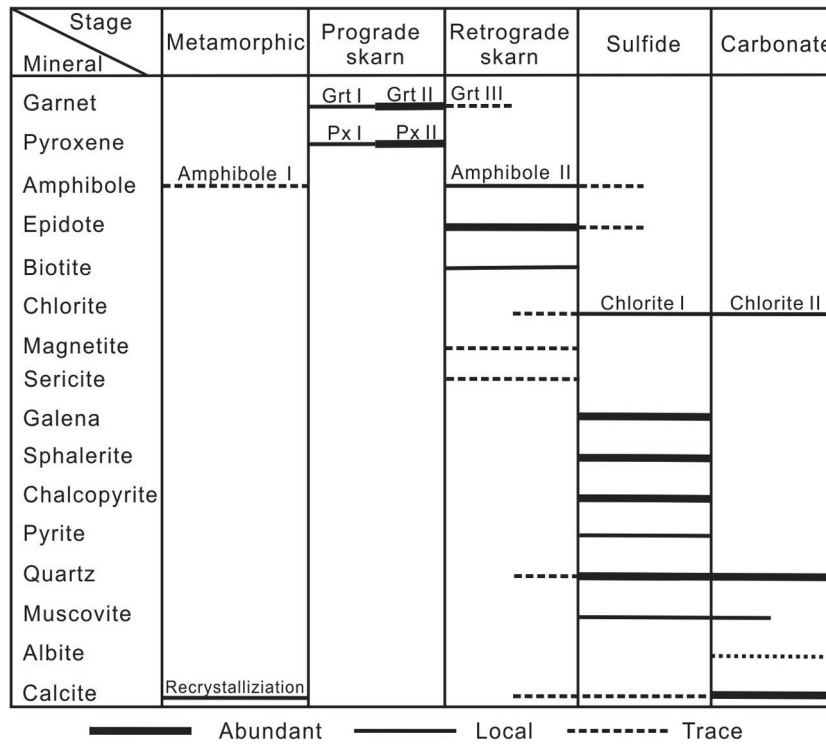


Fig. 6. Paragenetic sequence of the skarn minerals at Weibao.

amorphous aggregates replacing garnets and pyroxene in the banded skarn (Figs. 5g, h, 7g, h); (3) enveloped by sphalerite as epidote islands (Fig. 9e). The composition of epidote is less variable than that of garnet and pyroxene, and is Fe-rich with high Fe/(Fe + Mg) ratios ranging 0.26 to 0.49 (Table 3).

5.5. Amphibole

Amphibole at Weibao occurs either as (Amphibole I) poikilitic crystals in marble (Fig. 7a, i), or more commonly (Amphibole II) corroded garnet or pyroxene in skarn band, giving a spotted appearance in the banded skarn (Fig. 7h).

Amphibole I has a wide compositional range from actinolite to magnesio-hornblende, whilst Amphibole II is Mg-rich and belongs to actinolite with a narrow Mg/(Mg + Fe²⁺) range of 0.84 to 0.88 (Table 4; Fig. 10c).

5.6. Mica

Mica in the Weibao skarn consists of biotite and muscovite. Biotite flakes commonly replaced pyroxene or occurs as interstitials among pyroxene grains (Fig. 7g). Meanwhile, sulfides (e.g., galena) replaced biotite (Fig. 7g), suggesting that biotite was likely to have formed in the retrograde skarn stage. Muscovite occurs as fine flakes or patches, and generally coexists with galena by replacing garnet and pyroxene (Figs. 9f, 11a, b).

The Weibao biotite and muscovite are relatively homogeneous in composition (Table 5; Fig. 10d). According to the mica classification scheme (Foster, 1960), the Weibao biotite plots in the Mg-biotite field and muscovite in the muscovite field (Fig. 10d). As shown in the Fe³⁺-Fe²⁺-Mg ternary plot, the Weibao biotite shows low oxygen fugacity and plots close to the Ni-NiO buffer line (Fig. 10e).

5.7. Chlorite

The Weibao chlorite generally occurs as disseminated fine flakes. It was formed by replacing early-formed pyroxene and amphibole (Chlorite I) or as calcite + chlorite veins (Chlorite II) (Fig. 7j–l). Sporadically, chalcopyrite is associated with chlorite flakes (Chlorite I) and shows equilibrium boundaries with the latter (Fig. 7j). Chlorite I and II are virtually indistinguishable in composition, except for the slightly higher Al content of the latter (Table 6).

5.8. Sulfides

Galena and sphalerite are coeval and occur as patches or massive anhedral aggregates, which replaced skarn minerals or filled the interstices among skarn mineral grains (Figs. 5g, 7g, h, 8a–b). Locally, galena and sphalerite crosscut the banded skarn as veins (Figs. 5e, 7e) or intergrow with quartz to form massive ores (Fig. 8b). Pyrite is normally euhedral and usually enveloped by chalcopyrite but without replacing or crosscutting texture (Fig. 8c). Chalcopyrite is mainly disseminated in the skarn rocks and minor as exsolution blebs in sphalerite (Figs. 7j, 8d–f).

Sphalerite contains 4.61–6.88% Fe and 0.61–5.94% Cu, whilst galena has a small amount of Zn (0.03–0.82%) (Table 7).

5.9. Other minerals

Quartz is usually fine-grained and occurs as an alteration product of garnet and pyroxene in the banded skarn, or intergrows with sulfide minerals to form massive ores (Figs. 7g, 8b). In other places, quartz is present as late calcite + quartz veins cutting through the banded skarn (Fig. 7k, l). Hydrothermal calcite occurs mostly as garnet + sphalerite + galena + calcite veinlets or late calcite ± quartz ± chlorite veins (Fig. 7e, k, l).

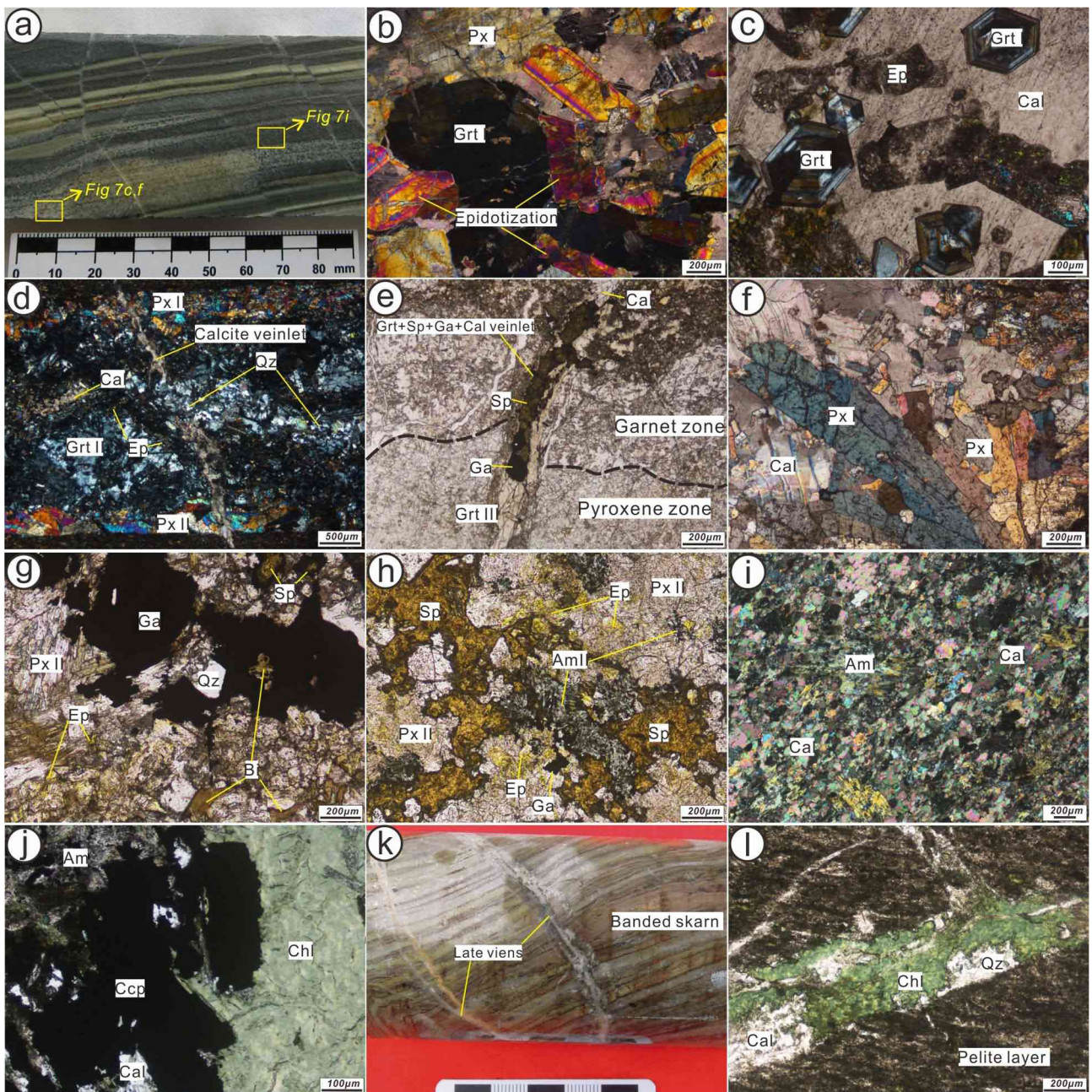


Fig. 7. Photomicrographs of the skarn minerals at Weibao. (a) Banded marble (gray) with chert interbed (beige). (b) Garnet (Grt I) and pyroxene (Px I) coexist in skarnized marble and were altered by epidote, showing pseudomorphic texture. (c) Speckled, euhedral, medium-grained garnets (Grt I) in skarnized marble. (d) Retrograde textures in banded skarn. Fine-grained quartz, calcite and epidote replaced garnet. Calcite veinlet crosscut banded skarn. (e) A garnet + sphalerite + galena + calcite veinlets crosscut pyroxene and garnet zones in the banded skarn. Note that sphalerite and galena replaced garnet in the vein. (f) Euhedral pyroxene monocrystals (Px I) in skarnized marble. (g) Biotite altered pyroxene or as interstitials among pyroxene grains. Epidote overprints pyroxene as amorphous yellow film on pyroxene surface. Galena and sphalerite coexist with quartz and replaced biotite-altered pyroxene. (h) Amphibole corroded pyroxene aggregate and is overprinted by galena and sphalerite. Epidote replaced pyroxene as fine-grained euhedral monocrystal or as amorphous yellow film on pyroxene surface. (i) Poikilitic amphibole in marble. (j) Chlorite replaced amphibole and associates with chalcopyrite. (k) Late veins crosscut banded skarn. (l) Late calcite + chlorite vein. Abbr: Grt, garnet; Px, pyroxene; Am, amphibole; Ep, epidote; Chl, Chlorite; Qz, quartz; Cal, calcite; Gn, Galena; Sp, sphalerite; Ccp, chalcopyrite.

6. Muscovite ^{40}Ar - ^{39}Ar chronology

6.1. Sampling and methodology

One syn-mineralization muscovite (intergrown with galena) was collected from the Weibao banded skarn (Fig. 11a, b). The sample was crushed to minus-20-mesh, from which the mica flakes were separated by conventional heavy liquid and magnetic separation techniques. The mica separates were cleaned in an

ultrasonic bath and 0.2 g of the mica flakes was handpicked under a binocular microscope.

Step-heating ^{40}Ar - ^{39}Ar measurements were carried out using an MM-1200 and GV Instruments 5400 mass spectrometer at the Ar-Ar Laboratory (GIGCAS), following the analytical procedures of Qiu and Wijbrans (2008). The muscovite separates, wrapped together (in Al foil and shielded with Cd foil) with the monitor standard DRA1 sanidine (recommended age: 25.26 ± 0.07 Ma), were irradiated with fast neutrons for 54 h at the Chinese Academy of Nuclear

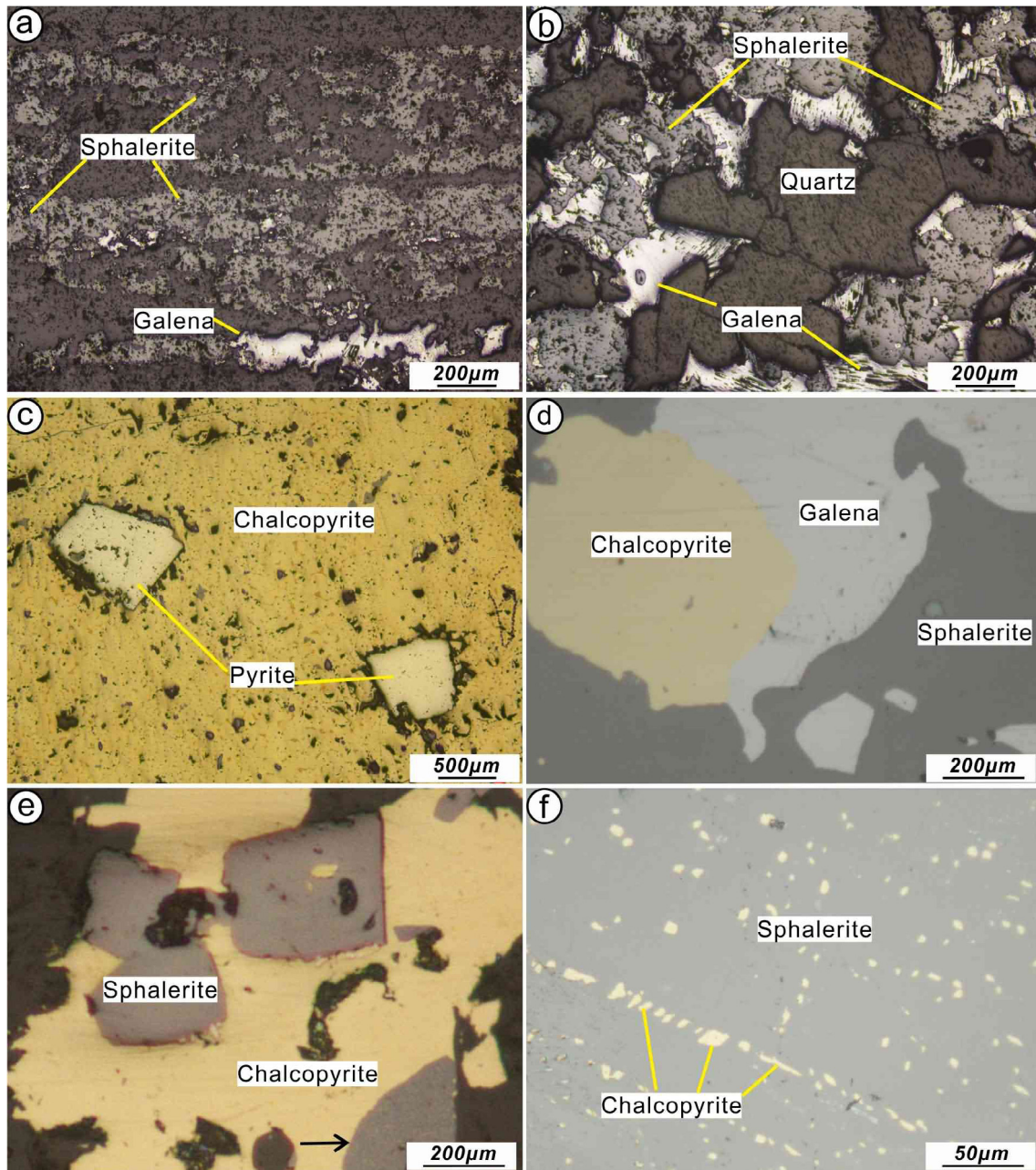


Fig. 8. Photomicrographs of sulfide minerals under reflected light. (a) Layered sphalerite and galena in the banded skarn. (b) Intergrowth of sphalerite, galena and quartz in massive ore. (c) Chalcopyrite envelopes euhedral pyrite. (d) Intergrowth of galena, sphalerite and chalcopyrite. (e) Intergrowth of sphalerite and chalcopyrite, showing equilibrium boundaries. Note the exsolution texture of chalcopyrite in sphalerite (black arrow). (f) Exsolution blebs of chalcopyrite in sphalerite.

Energy Sciences (Beijing). Correction factors for interfering Ar isotopes derived from Ca and K are: $(^{39}\text{Ar}/^{37}\text{Ar})\text{Ca} = 8.984 \times 10^{-4}$, $(^{36}\text{Ar}/^{37}\text{Ar})\text{Ca} = 2.673 \times 10^{-4}$ and $(^{40}\text{Ar}/^{39}\text{Ar})\text{K} = 5.97 \times 10^{-3}$. The sample was crushed in a 210×28 mm (in bore diameter) high-temperature resistant stainless steel tube ($T_{\text{max}} = 1200^\circ\text{C}$). The extraction and purification lines were baked out for about 10 h at 150°C using a heating tape and the crusher at 250°C using an external tube furnace. The blanks are: ^{36}Ar (0.002–0.004) mV, ^{37}Ar (0.0002–0.0006) mV, ^{38}Ar (0.0004–0.0015) mV, ^{39}Ar (0.0025–0.0051) mV, and ^{40}Ar (0.51–1.3) mV. The released gas was purified for 5–8 min by two Zr/Al getter pumps operating at room temperature and $\sim 450^\circ\text{C}$. The $^{40}\text{Ar}/^{39}\text{Ar}$ results were calculated and plotted using the ArArCALC software (Koppers, 2002). Plateau, isochron and inverse isochron ages were given at 2σ

confidence level. The uncertainties on the $^{40}\text{Ar}/^{39}\text{Ar}$ ratios of the monitors were included in the calculation of the integrated and plateau age uncertainties, but the error on the monitor age was not included.

6.2. Results

The composition of mica and calculated molecular formula were listed in Table 6. EMPA data suggested that the analyzed mica is muscovite (Deer et al., 1997) with a molecular formula of $(\text{K}_{0.92}, \text{Na}_{0.06}, \text{Ca}_{0.02})_{1.00}(\text{Al}_{1.69}, \text{Fe}^{3+}_{0.18}, \text{Mg}_{0.02}, \text{Ti}_{0.01})_{1.89}[(\text{Si}_{3.08}, \text{Al}_{0.92})_{1.00}(\text{OH}_{2.00}, \text{Cl}_{0.01})_2]$.

The $^{40}\text{Ar}-^{39}\text{Ar}$ dating results were listed in Table 8, and the corresponding plateau age and isochron age were plotted in

Table 1

Representative electron microprobe data of garnets from the Weibao deposit.

Sample	WBY3-34-1			Garnet I			WBY3-34-2			Garnet I			WBY3-31			Garnet I	WBY3-24			Garnet II	N = 10	WBY3-25			Garnet II	N = 10
	Core	Middle	Rim	Core	Middle	Rim	Core	Rim	Maximum	Minimum	Average	Maximum	Minimum	Average	Core	Maximum	Minimum	Average	Core	Maximum	Minimum	Average	Core	Maximum	Minimum	Average
SiO ₂	33.62	34.59	33.72		34.06	32.98	33.08		33.10	34.24	34.60	34.12	34.60	33.03	34.73											
TiO ₂	0.00	0.48	0.00	0.52	0.57	0.50	0.00	0.72	0.02	0.14	0.20	0.14	0.00	0.09												
Al ₂ O ₃	0.05	15.01	0.06	14.54	14.02	13.53	0.04	13.54	13.54	16.65	9.11	16.65	0.45	8.97												
Cr ₂ O ₃	0.00	0.00	0.00	0.00	0.00	0.00	0.00	0.00	0.00	0.00	0.00	0.00	0.00	0.00												
FeO	28.65	11.07	28.25	11.66	12.10	12.98	28.05	12.73	12.96	9.43	17.98	9.43	28.06	18.24												
MnO	0.41	0.42	0.23	0.19	0.10	0.32	0.07	0.36	0.52	0.73	0.61	0.73	0.28	0.33												
MgO	0.03	0.00	0.03	0.02	0.01	0.03	0.03	0.01	0.03	0.01	0.03	0.01	0.07	0.04												
CaO	34.48	37.03	34.67	37.40	37.22	36.71	34.47	37.16	36.45	37.12	35.53	37.12	34.86	35.36												
Total	97.23	98.60	96.96	98.06	98.07	97.06	95.73	97.62	97.74	98.69	97.57	98.69	96.74	97.76												
Number of cation on the basis of 12 oxygen atoms and garnet end-member normative calculation																										
Si	2.87	2.76	2.88	2.72	2.74	2.70	2.87	2.70	2.77	2.87	2.81	2.75	2.84	2.85												
Ti	0.00	0.03	0.00	0.03	0.03	0.03	0.00	0.04	0.00	0.00	0.01	0.01	0.00	0.01												
Al	0.01	1.41	0.01	1.38	1.33	1.31	0.00	1.30	1.29	0.03	0.88	1.56	0.05	0.85												
Cr	0.00	0.00	0.00	0.00	0.00	0.00	0.00	0.00	0.00	0.00	0.00	0.00	0.00	0.00												
Fe ³⁺	2.04	0.73	2.02	0.78	0.82	0.87	2.03	0.87	0.86	2.00	1.23	0.60	2.02	1.24												
Fe ²⁺	0.00	0.01	0.00	0.00	0.00	0.02	0.00	0.00	0.02	0.00	0.01	0.03	0.00	0.03												
Mn	0.03	0.03	0.02	0.01	0.01	0.02	0.00	0.02	0.04	0.03	0.04	0.05	0.02	0.02												
Mg	0.00	0.00	0.00	0.00	0.00	0.00	0.00	0.00	0.00	0.01	0.00	0.01	0.00	0.00												
Ca	3.15	3.17	3.18	3.23	3.21	3.22	3.20	3.24	3.17	3.17	3.13	3.16	3.21	3.11												
Ad	96	34	95	36	38	40	96	40	40	93	58	28	93	59												
Sp	1	1	0	0	0	1	0	1	1	1	1	2	1	1												
Gr	3	65	5	63	62	59	4	59	58	5	40	70	6	40												
Sample	WBY3-15 Maximum	Garnet II Minimum	N=11 Average	WBY3-21 Maximum	Garnet II Minimum	N=9 Average	WBY3-17 WBY3-17-1	WBY3-17-2	WBY3-17-3	WBY3-17-4	WBY3-17-5	Garnet III Average														
SiO ₂	37.14	33.57	35.19	35.79	33.46	34.74	36.36	35.93	31.46	31.97	34.32	34.01														
TiO ₂	0.03	0.00	0.03	0.54	0.00	0.20	0.43	0.62	0.72	0.63	0.72	0.62														
Al ₂ O ₃	17.70	0.16	9.66	15.24	0.94	9.76	17.67	9.56	9.80	9.07	7.89	10.80														
Cr ₂ O ₃	0.00	0.00	0.00	0.00	0.00	0.00	0.00	0.00	0.00	0.00	0.00	0.00														
FeO	8.87	28.53	17.32	11.02	27.17	17.00	5.56	18.35	16.32	17.00	16.45	14.74														
MnO	0.43	0.15	0.29	0.17	0.19	0.26	1.48	1.89	2.08	1.73	2.45	1.92														
MgO	0.01	0.05	0.02	0.01	0.03	0.03	0.01	0.02	0.02	0.01	0.03	0.02														
CaO	36.32	34.15	34.92	36.51	34.15	34.99	36.32	34.15	36.48	34.86	32.75	34.91														
Total	100.49	96.61	97.44	99.28	95.95	96.97	97.83	100.52	96.88	95.26	94.60	97.02														
Number of cation on the basis of 12 oxygen atoms and garnet end-member normative calculation																										
Si	2.87	2.88	2.88	2.82	2.88	2.86	2.88	2.86	2.65	2.72	2.91	2.80														
Ti	0.00	0.00	0.00	0.03	0.00	0.01	0.03	0.04	0.05	0.04	0.05	0.04														
Al	1.61	0.02	0.90	1.42	0.10	0.93	1.65	0.90	0.97	0.91	0.79	1.04														
Cr	0.00	0.00	0.00	0.00	0.00	0.00	0.00	0.00	0.00	0.00	0.00	0.00														
Fe ³⁺	0.48	2.04	1.17	0.68	1.96	1.15	0.37	1.17	1.15	1.21	1.17	1.01														
Fe ²⁺	0.10	0.00	0.04	0.05	0.00	0.04	0.00	0.05	0.00	0.00	0.00	0.01														
Mn	0.03	0.01	0.02	0.01	0.01	0.02	0.10	0.13	0.15	0.12	0.18	0.13														
Mg	0.00	0.01	0.00	0.00	0.00	0.00	0.00	0.00	0.00	0.00	0.00	0.00														
Ca	3.00	3.14	3.06	3.09	3.15	3.08	3.08	2.92	3.29	3.18	2.98	3.09														
Ad	23	97	56	32	93	55	17	57	50	55	55	47														
Sp	1	0	1	0	0	1	3	4	4	4	4	4														
Gr	73	2	42	66	7	43	80	37	46	41	39	49														

Note: Maximum represents the grossularite-richest garnets; Minimum represents the andradite-richest garnets.

Fig. 11c, d. The muscovite yielded an ^{40}Ar - ^{39}Ar apparent age of 224.53 ± 2.15 Ma defined by all the 17 stages of gas emissions and a plateau age of 226.61 ± 2.34 Ma covering the 8th to 13th heating stages, with a normal isochron age of 223.20 ± 3.93 Ma and an inverse isochron age of 223.27 ± 3.95 Ma. The plateau age, normal isochron age and isochron age were consistent within the analytical error, suggesting the dating is reliable.

7. Discussion

7.1. Formation of the Weibao banded skarn

Centimeter-scale banded skarn was proposed to have formed via bimetasomatism (Frantz and Mao, 1976; Kwak, 2012; Meinert et al., 2005; Thompson, 1975). Bimetasomatic skarn generally occurs along the contact of marble and Si-Al units (mainly granites), and is caused by thermal metamorphism. Major bimetaso-

matic chemical activities involve component exchange between marble and Si-Al units, i.e., SiO₂ diffuses into the marble and Ca into the Si-Al units, forming the small-scale banded skarn. The major drives for these reactions are the chemical potential gradients in response to the temperature or possibly pressure changes (Kwak, 2012).

Some other workers argued that the banded skarn may have formed as isochemically metamorphosed calc-silicate-rich submarine exhalative beds, induced by intrusion-related thermal metamorphism or regional metamorphism (Barnes, 1983; Liu et al., 2012; Newberry et al., 1986; Oen et al., 1986). In brief, the banding in the skarn may have been inherited sedimentary structures. These skarn bands are characterized by well-developed mineral foliation, lack of sulfide veining and a unique calc-silicate mineral composition such as spessartine-rich garnet (Appendix B; Fig. 10a, b) (Barnes, 1983; Newberry et al., 1986; Pertoldova et al., 2009).

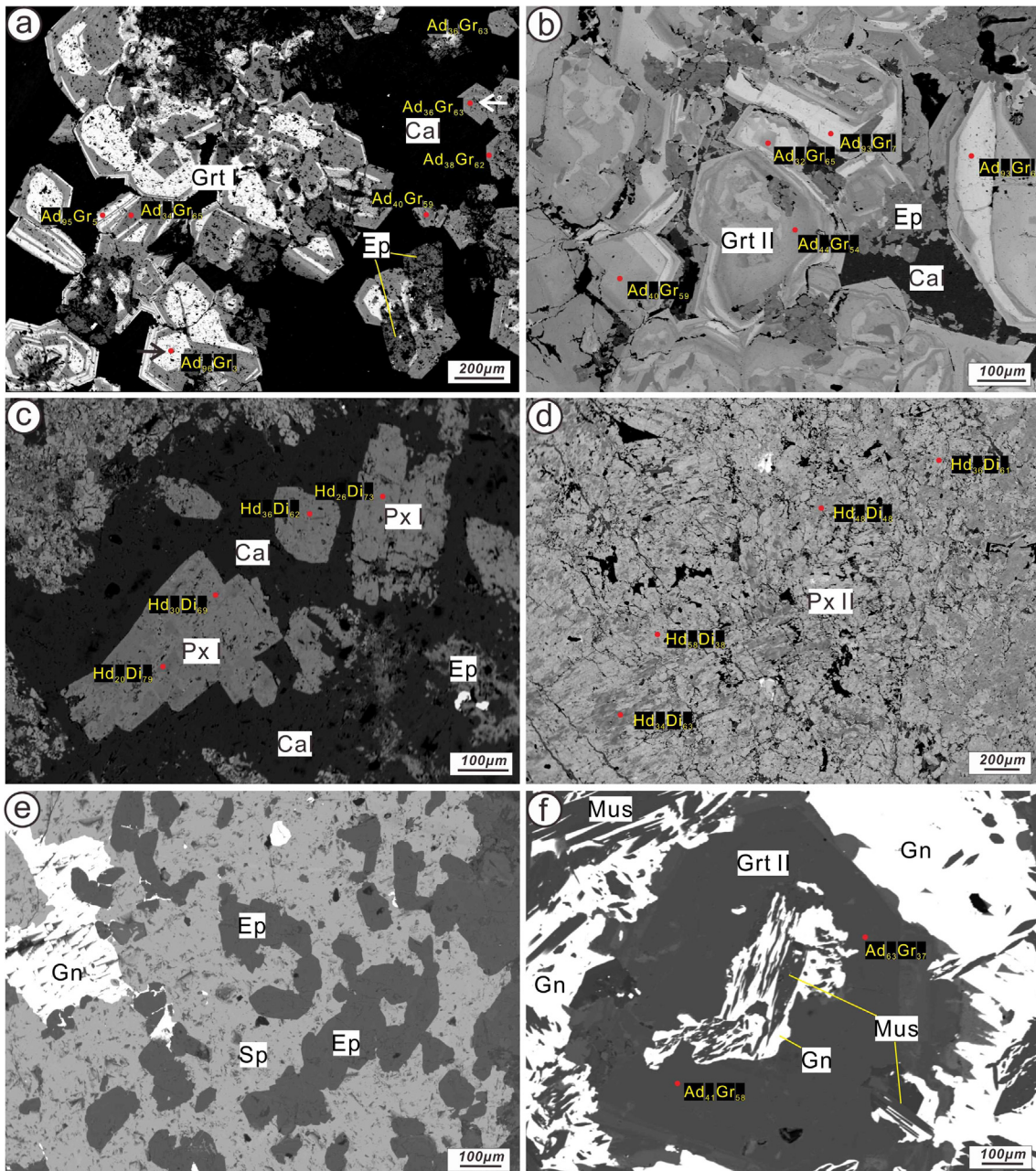


Fig. 9. BSE images of the Weibao skarn minerals. (a) Speckled, euhedral, medium-grained garnet (Grt I) in skarnized marble. These garnet grains have andradite-enriched core and grossularite-rich rim (black arrow), or are compositionally homogeneous and grossularite-rich. (b) Garnet aggregates (Grt II) in banded skarn with heterogeneous composition. (c) Isolated, euhedral, pyroxene monocrystals (Px I) in skarnized marble, with minor epidote. (d) Pyroxene aggregates (Px II) in banded skarn. (e) Galena and sphalerite replaced epidote, showing an “island” texture of epidote. (f) Galena and muscovite intergrowth replaced Garnet. Abbr: Grt, garnet; Px, pyroxene; Ep, epidote; Qz, quartz; Cal, calcite; Sp, sphalerite.

However, neither of above-mentioned genetic models can fully explain the formation of banded skarn at Weibao. First, no intrusive rocks or endoskarn were found near the Weibao orebodies, meaning an absence of heat source to drive the bimetamorphic skarn formation. Additionally, in the Weibao banded skarn, the epitaxial pyroxene veins from the pyroxene zone commonly cut through the pelite layers, resembling typical hydrothermal metasomatism rather than thermal metamorphism (Fig. 5a, d). In bimetamorphic skarn, the garnet is mainly grossularitic and wollastonite is commonly present (Calagari and Hosseinzadeh, 2006; Thompson, 1975), yet garnet in the Weibao banded skarn belongs to the grossularite-andradite solution series and wollastonite is rare. The metamorphosed submarine exhalative model is also unli-

kely to be applicable to the Weibao case either: In order to produce skarn minerals, especially garnet and pyroxene, the metamorphic peak condition should reach eclogite facies (Pertoldova et al., 2009 and references therein), yet no eclogite-facies rocks are exposed at or around Weibao. Skarn rocks generated by regional metamorphism always show metamorphic textures and structures like foliation texture, phyllosilicate cleavage structure and radiating pattern of garnet grains (Barnes, 1983; Newberry et al., 1986; Pertoldova et al., 2009), which are all absent in the Weibao banded skarn. More importantly, regional metamorphic skarn rocks commonly contain metamorphic minerals such as garnatite, cordierite, grunerite and kyanite (Barnes, 1983; Pertoldova et al., 2009), which are again all absent in the Weibao skarn rocks. Furthermore,

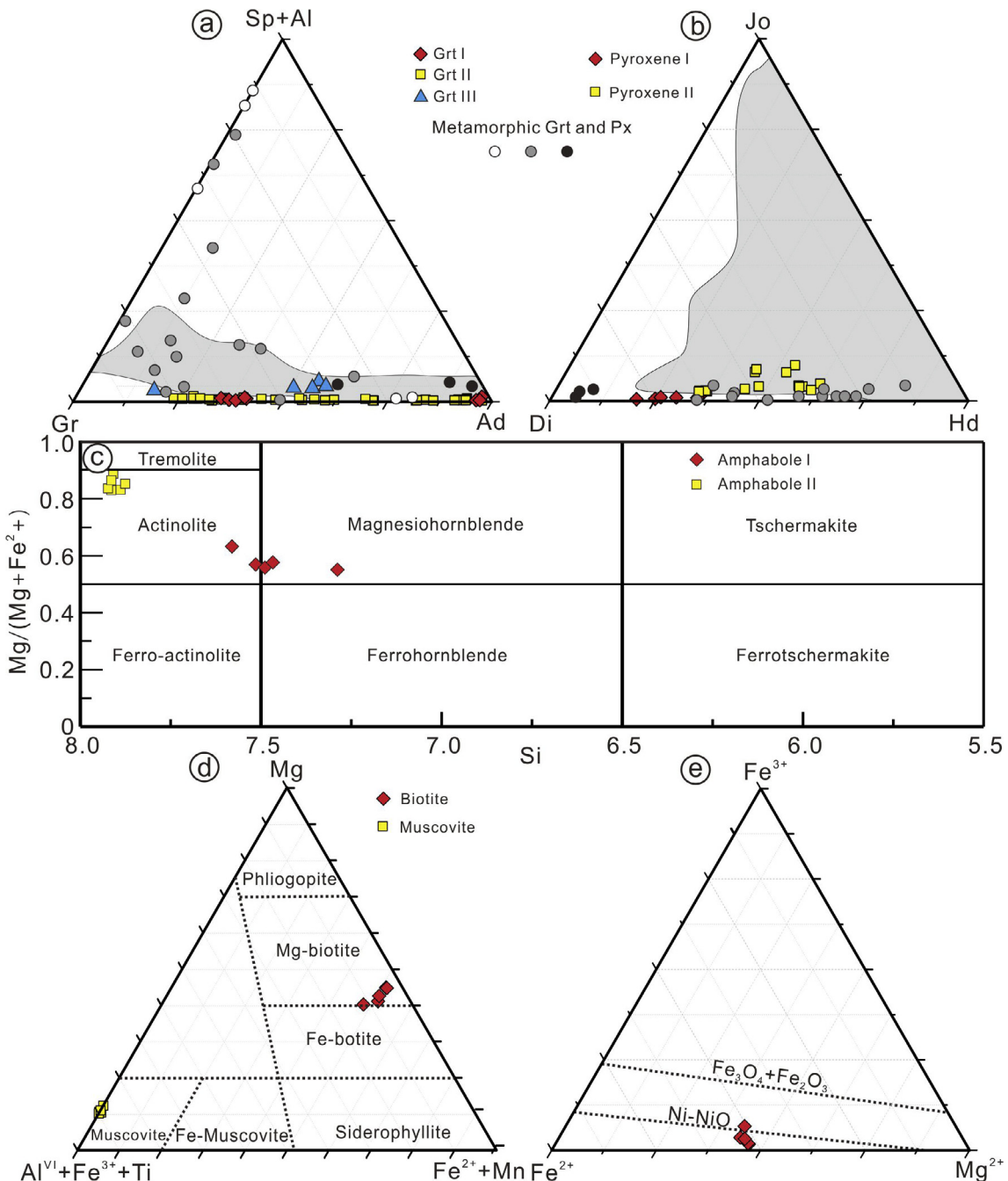


Fig. 10. (a) and (b) Ternary plots of the Weibao garnet and pyroxene compositions, in comparison with those of the skarn Zn deposits worldwide (shaded area; after Meinert et al., 2005); Circles represent the garnet and pyroxene in skarn formed via regional metamorphism. Data sources: White circles (Newberry et al., 1986), gray circles (Pertoldova et al., 2009), black circles (Stanton, 1989). (c) Compositional classification of amphibole from the Weibao skarn (after Leake et al., 2004). (d) Compositional classification of mica from the Weibao skarn (after Foster, 1960). (e) Oxygen fugacity of biotite from the Weibao skarn (after Wones and Eugster, 1965).

fluid inclusion studies also suggested that the Weibao skarn minerals contain fluid inclusions mimicking magmatic fluids, not metamorphic ones (Fang et al., 2015).

The Weibao banded skarn is more likely to have a hydrothermal metasomatic genesis and can be viewed as a distal skarn system, where the morphologic and mineralogical characters of the skarn are mainly determined by the host rocks rather than the associated intrusive rocks. At Weibao, magmatic fluids may have experienced long distance migration and become incapable of totally assimilating the host rocks. Instead, the fluids may have infiltrated along boundaries between the carbonate and pelitic layers. In this scenario, magmatic fluids are likely to have low filtration velocity and limited material replenishment. The geochemistry and ambi-

ent conditions under which skarn minerals are formed are mainly determined by the host rocks (instead of the magmatic fluids). The compositional differences between the marble and pelitic layers may have created spatial oscillations in the compositions and physicochemical conditions of the ore fluids (Guy, 1993; Rusinov and Zhukov, 2008). Specifically, the ore fluids produced by the reaction between the magmatic fluids and pelitic layers have had higher SiO₂ content and were more reduced, as inferred from the high SiO₂ (up to 40 wt%) and the presence of organic matter in the pelitic layers, while the ore fluids formed by the reaction between the magmatic fluids and marble layers have had higher CaO and were more oxidized than the pelitic layers. Garnet is depleted in SiO₂ and enriched in CaO compared to pyroxene, thus

Table 2

Representative electron microprobe data of pyroxenes from the Weibao deposit.

Sample	WBY3-34 Maximum	Pyroxene I Minimum	n = 6 Average	WBY3-24 Maximum	Pyroxene II Minimum	n = 8 Average	WBY3-25 Maximum	Pyroxene II Minimum	n = 9 Average	WBY3-15 Maximum	Pyroxene II Minimum	n = 10 Average
SiO ₂	52.82	51.57	52.43	50.91	50.34	50.73	52.59	50.73	52.31	52.95	50.92	52.27
TiO ₂	0.00	0.00	0.00	0.03	0.01	0.01	0.01	0.00	0.01	0.00	0.00	0.01
Al ₂ O ₃	0.22	0.06	0.14	0.06	0.05	0.06	0.00	0.04	0.03	0.00	0.04	0.02
Cr ₂ O ₃	0.38	0.01	0.08	0.02	0.00	0.00	0.00	0.00	0.00	0.00	0.00	0.01
FeO	7.20	12.30	9.95	13.96	18.32	16.30	11.14	18.14	13.41	11.01	16.48	14.38
MnO	0.16	0.72	0.34	2.31	1.29	1.71	0.81	0.83	0.87	0.74	3.17	1.40
MgO	13.53	10.25	12.01	8.02	5.78	6.94	11.04	6.22	9.39	10.98	6.06	8.62
CaO	25.57	25.21	25.18	23.30	23.11	23.11	24.39	23.38	24.06	24.64	23.07	23.79
Na ₂ O	0.13	0.05	0.08	0.06	0.03	0.05	0.03	0.05	0.04	0.02	0.05	0.04
Total	100.03	100.19	100.22	98.66	98.93	98.90	100.01	99.39	100.12	100.33	99.80	100.53
Number of cation on the basis of 6 oxygen atoms and pyroxene end-member normative calculation												
Si	1.98	1.98	1.98	2.00	2.01	2.00	2.00	2.01	2.01	2.00	2.01	2.01
Al(IV)	0.00	0.00	0.00	0.00	0.00	0.00	0.00	0.00	0.00	0.00	0.00	0.00
Al(vi)	0.00	0.00	0.00	0.00	0.00	0.00	0.00	0.00	0.00	0.00	0.00	0.00
Ti	0.00	0.00	0.00	0.00	0.00	0.00	0.00	0.00	0.00	0.00	0.00	0.00
Cr	0.01	0.00	0.00	0.00	0.00	0.00	0.00	0.00	0.00	0.00	0.00	0.00
Fe ³⁺	0.05	0.07	0.05	0.00	0.00	0.00	0.00	0.00	0.00	0.00	0.00	0.00
Fe ²⁺	0.17	0.32	0.26	0.46	0.61	0.54	0.35	0.60	0.43	0.35	0.54	0.46
Mn	0.01	0.02	0.01	0.08	0.04	0.06	0.03	0.03	0.03	0.02	0.11	0.05
Mg	0.75	0.59	0.68	0.47	0.34	0.41	0.63	0.37	0.54	0.62	0.36	0.49
Ca	1.03	1.04	1.02	0.98	0.99	0.98	0.99	0.99	0.99	1.00	0.97	0.98
Na	0.01	0.00	0.01	0.00	0.00	0.00	0.00	0.00	0.00	0.00	0.00	0.00
Hd	20	36	29	45	62	54	34	61	43	35	55	46
Jo	1	2	1	9	5	6	3	3	3	2	13	5
Di	79	62	70	46	33	40	63	36	54	63	32	48

Table 3

Representative electron microprobe data of epidotes from the Weibao deposit.

Sample	WBY3-9-1	WBY3-9-2	WBY3-24-1	WBY3-24-2	WBY3-25-1	WBY3-25-2	WBY3-25-3	WBY3-15-1	WBY3-15-2	WBY3-15-3	WBY3-31-1	WBY3-31-2	WBY3-31-3
K ₂ O	0.01	0.01	0.05	0.00	0.01	0.00	0.01	0.01	0.00	0.01	0.01	0.01	0.00
TiO ₂	0.05	0.00	0.10	0.09	0.13	0.14	0.04	0.15	0.14	0.04	0.15	0.20	0.12
Na ₂ O	0.00	0.02	0.00	0.00	0.01	0.04	0.03	0.02	0.04	0.03	0.02	0.02	0.04
CaO	24.00	24.64	23.82	24.95	24.26	22.69	22.65	22.47	22.69	22.65	22.47	22.77	22.49
Al ₂ O ₃	21.47	24.38	23.58	24.98	22.70	22.99	24.84	20.90	22.99	24.84	20.90	22.56	21.07
FeO	13.34	9.67	10.11	9.27	10.14	11.07	9.16	14.53	11.07	9.16	14.53	12.09	13.67
SiO ₂	36.95	37.63	37.56	38.42	36.66	37.80	38.27	37.75	37.80	38.27	37.75	37.64	37.57
MnO	0.06	0.00	0.08	0.02	0.04	0.17	0.00	0.07	0.17	0.00	0.07	0.18	0.04
MgO	0.05	0.01	0.32	0.01	0.03	0.04	0.03	0.02	0.04	0.03	0.02	0.04	0.01
Total	95.92	96.35	95.60	97.73	93.97	94.93	95.03	95.92	94.93	95.03	95.92	95.51	95.02
Number of cation on the basis of 12.5 oxygen atoms													
K	0.00	0.00	0.00	0.00	0.00	0.00	0.00	0.00	0.00	0.00	0.00	0.00	0.00
Ti	0.00	0.00	0.01	0.01	0.01	0.01	0.00	0.01	0.01	0.00	0.01	0.01	0.01
Na	0.00	0.00	0.00	0.00	0.00	0.01	0.01	0.00	0.01	0.01	0.00	0.00	0.01
Ca	2.07	2.09	2.04	2.09	2.12	1.97	1.95	1.95	1.97	1.95	1.95	1.97	1.96
Al	2.04	2.28	2.22	2.30	2.18	2.19	2.35	1.99	2.19	2.35	1.99	2.15	2.02
Fe ³⁺	0.90	0.64	0.68	0.61	0.69	0.75	0.61	0.98	0.75	0.61	0.98	0.82	0.93
Si	2.98	2.98	3.01	3.00	2.99	3.06	3.07	3.05	3.06	3.07	3.05	3.04	3.06
Mn	0.00	0.00	0.01	0.00	0.00	0.01	0.00	0.01	0.00	0.00	0.01	0.00	0.00
Mg	0.01	0.00	0.04	0.00	0.00	0.00	0.00	0.00	0.00	0.00	0.00	0.01	0.00
Fe/(Fe + Al)	0.44	0.28	0.30	0.26	0.32	0.34	0.26	0.49	0.34	0.26	0.49	0.38	0.46

the garnet zones are formed close to the marble layers whilst the pyroxene zones close to the pelite layers, creating the embryo of the banded skarn (Guy, 1993; Kwak, 2012). Dissolution of the marble layers can also provide CaO to pyroxene, which is reason why pyroxene near the garnet zones (originally marble layers) is coarser than that in the pelitic layers (Fig. 5d, e). Pelite dissolution can supply Al₂O₃ for the garnet formation, and hence garnet in the banded skarn tends to be grossular-rich. The banded skarn formation may have been an example of geochemical self-organization in a disequilibrium system, where garnet and pyroxene compete for space and mineral-forming ingredients (Ciobanu and Cook, 2004; Guy, 1993; L'Heureux, 2013; Ortoleva et al., 1987; Rusinov and Zhukov, 2008). Disequilibrium of the Weibao skarn system has been well-reflected by the heterogeneous garnet internal composition of the banded skarn (Figs. 5c, 7d, 9b).

7.2. Nature of hydrothermal fluids and ore genesis

The three garnet types (Garnet I, II and III) and two pyroxene type (Pyroxene I and II) in the Weibao skarn were all likely to form by hydrothermal metasomatism. Garnet I and Pyroxene I were likely to have formed at the early magma crystallization, when magmatic fluids had not been totally exsolved from the magma and only a small volume of volatile-rich fluids were generated (Fig. 12c; Meinert et al., 2003; Peng et al., 2015). These fluids were acidic and high temperature, and they reacted with the marble inside the carbonate pore space. Probably owing to the sufficient mineral-forming ingredient supply and growth space, Garnet I is euhedral and relatively homogeneous in composition (Fig. 7a-c, 9a), which (together with the grossular-rich nature) also suggests a high-temperature and low W/R ratios formation environment.

Table 4

Representative electron microprobe data of amphiboles from the Weibao deposit.

Sample	WBY3-34			Amphibole I		WBY3-15				Amphibole II		
	WBY3-31-1	WBY3-31-2	WBY3-31-3	WBY3-31-4	WBY3-31-5	WBY3-15-1	WBY3-15-2	WBY3-15-3	WBY3-17-1	WBY3-17-2	WBY3-17-3	
SiO ₂	51.34	50.28	48.26	50.11	50.09	54.61	55.17	54.23	54.70	53.95	55.27	
TiO ₂	0.05	0.07	0.20	0.05	0.02	0.01	0.00	0.00	0.00	0.00	0.01	
Al ₂ O ₃	3.72	4.45	6.23	4.51	4.76	1.30	0.84	1.42	1.12	1.56	1.52	
FeO	18.38	20.05	19.58	20.44	19.60	12.77	12.91	12.95	12.85	11.94	12.08	
MnO	0.25	0.24	0.30	0.27	0.26	1.11	1.12	1.06	1.17	1.22	1.01	
MgO	11.15	9.83	9.38	9.83	10.06	15.45	15.17	14.93	14.98	15.19	15.51	
CaO	12.87	12.40	12.25	12.32	12.58	12.35	12.71	12.35	12.58	12.23	12.62	
Na ₂ O	0.38	0.37	0.56	0.38	0.48	0.22	0.12	0.22	0.16	0.27	0.21	
K ₂ O	0.14	0.14	0.29	0.12	0.16	0.09	0.02	0.06	0.07	0.06	0.02	
Total	98.27	97.84	97.05	98.02	98.01	97.91	98.06	97.22	97.64	96.41	98.25	
Number of cation on the basis of 23 oxygen atoms												
Si	7.58	7.51	7.29	7.49	7.47	7.87	7.93	7.87	7.91	7.87	7.89	
AlIV	0.42	0.49	0.71	0.51	0.53	0.13	0.07	0.13	0.09	0.13	0.11	
AlVI	0.23	0.30	0.40	0.28	0.30	0.09	0.08	0.11	0.10	0.14	0.15	
Ti	0.01	0.01	0.02	0.01	0.00	0.00	0.00	0.00	0.00	0.00	0.00	
Fe ³⁺	0.84	0.85	0.76	0.83	0.80	0.94	0.99	0.96	0.97	0.96	0.99	
Fe ²⁺	1.43	1.66	1.72	1.73	1.64	0.60	0.57	0.62	0.58	0.50	0.45	
Mn	0.03	0.03	0.04	0.03	0.03	0.14	0.14	0.13	0.14	0.15	0.12	
Mg	2.45	2.19	2.11	2.19	2.24	3.32	3.25	3.23	3.23	3.30	3.30	
Ca	2.04	1.99	1.98	1.97	2.01	1.91	1.96	1.92	1.95	1.91	1.93	
Na	0.11	0.11	0.17	0.11	0.14	0.06	0.03	0.06	0.04	0.08	0.06	
K	0.03	0.03	0.06	0.02	0.03	0.02	0.00	0.01	0.01	0.01	0.00	
Total	15.16	15.15	15.24	15.17	15.20	15.06	15.01	15.04	15.03	15.04	15.01	
SiT ⁺	7.58	7.51	7.29	7.49	7.47	7.87	7.93	7.87	7.91	7.87	7.89	
AlT	0.42	0.49	0.71	0.51	0.53	0.13	0.07	0.13	0.09	0.13	0.11	
AlC	0.23	0.30	0.40	0.28	0.30	0.09	0.08	0.11	0.10	0.14	0.15	
Fe ³⁺ C	0.84	0.85	0.76	0.83	0.80	0.94	0.99	0.96	0.97	0.96	0.99	
TiC	0.01	0.01	0.02	0.01	0.00	0.00	0.00	0.00	0.00	0.00	0.00	
MgC	2.45	2.19	2.11	2.19	2.24	3.32	3.25	3.23	3.23	3.30	3.30	
Fe ²⁺ C	1.43	1.66	1.71	1.70	1.64	0.60	0.57	0.62	0.58	0.50	0.45	
MnC	0.03	0.00	0.00	0.00	0.01	0.06	0.12	0.08	0.12	0.11	0.11	
Fe ²⁺ B	0.00	0.00	0.00	0.03	0.00	0.00	0.00	0.00	0.00	0.00	0.00	
MnB	0.00	0.03	0.04	0.03	0.02	0.08	0.02	0.05	0.02	0.04	0.02	
CaB	2.00	1.97	1.96	1.93	1.98	1.91	1.96	1.92	1.95	1.91	1.93	
NaB	0.00	0.00	0.00	0.00	0.00	0.02	0.02	0.03	0.03	0.05	0.05	
CaA	0.04	0.02	0.02	0.04	0.03	0.00	0.00	0.00	0.00	0.00	0.00	
NaA	0.11	0.11	0.17	0.11	0.14	0.05	0.01	0.03	0.01	0.03	0.01	
KA	0.03	0.03	0.06	0.02	0.03	0.02	0.00	0.01	0.01	0.01	0.00	
Mg/(Mg + Fe ²⁺)	0.63	0.57	0.55	0.56	0.58	0.85	0.85	0.84	0.85	0.87	0.88	

ment (Dietvorst, 1982). In addition, Garnet I has generally andradite-rich cores and Pyroxene I is diopside-rich (Figs. 9a, c, 10a, b). These features, together with the extensive epidote alteration, indicate that the initial Weibao ore fluids were oxidized (Lu et al., 2003; Meinert et al., 2005).

Garnet II and Pyroxene II occur in banded skarn and volumetrically dominate the skarn mineral assemblages. Associated with the further magmatic fractionation, a larger amount of magmatic metal- and volatile-rich fluids may have exsolved (Fig. 12d; Meinert et al., 2003). These hydrothermal fluids would have migrated for a long distance along faults or other permeable zones before they reacted with impure limestone of the Langyashan Formation (Fig. 12d). Subsequently, Garnet II and Pyroxene II were formed by infiltrative metasomatism between argillaceous limestone and magmatic fluids in a disequilibrated geochemical system as discussed above.

Garnet III occurs as garnet + sphalerite + galena + calcite veinlets crosscutting the banded pyroxene and garnet layers (Fig. 7e). These garnet grains are grossular-rich but have higher Mn than Garnet I and II (Fig. 10a). Garnet III was inferred to be formed under lower temperature than Garnet I and II. We interpreted that the Garnet III-bearing veinlets were products of multiple hydrothermal pulses, which are highly common in skarn mineralization.

Fluid inclusion studies suggest that precipitation of the Weibao sulfides was caused by gradual reactions between the magmatic fluids and host rocks (Fang et al., 2015). This argument is supported by our mineralogical studies: The Weibao sulfides precipitated mainly

through replacing anhydrous and hydrous minerals or as interstitials and minor as galena + sphalerite veins. Consequently, the sulfide precipitation may be controlled chiefly by the ore fluid physicochemical conditions and the early-formed skarn minerals that reacted with the fluids. For the former case, sulfide precipitation was favored by a temperature and f_{O_2} decrease. Decrease in temperature would lower the solubility of metal-chlorine complexes, while f_{O_2} decrease would reduce their stability and promote the sulfide precipitation (Barnes, 1997; Robb, 2009). At Weibao skarn, decrease in f_{O_2} may be caused by extensive retrograde epidote alteration, which consumes Fe³⁺ and caused the f_{O_2} decrease in the following sulfide stage (Calagari and Hosseinzadeh, 2006). The relatively low f_{O_2} of the Weibao biotite (Fig. 10e) also reflects the consumption of Fe³⁺ by the epidote alteration. For the latter case, the sulfide layering (Figs. 4b, 5a, b, 8a) was likely inherited from the banded skarn. Sulfide minerals preferentially replaced pyroxene rather than garnet in the banded skarn, as the mobility of Fe²⁺ and Mg is higher than Al in the hydrothermal system, making pyroxene more vulnerable to alteration (Meinert et al., 2005).

7.3. Mineralization age and geodynamic setting

Mica $^{40}\text{Ar}/^{39}\text{Ar}$ dating is an effective and common method to date hydrothermal mineralization, as mica is a common gangue mineral and has relatively high closure temperature ($>350\text{ }^{\circ}\text{C}$; Harrison et al., 1985). At Weibao, muscovite coexists with galena and sphalerite in the banded skarn (Figs. 9f, 11a, b). Besides, according to

Table 5

Representative electron microprobe data of micas from the Weibao deposit.

Sample	WBY3-15	WBY3-15-1	WBY3-15-2	WBY3-15-3	WBY3-15-4	Biotite	WBY3-21	WBY3-21-1	WBY3-21-2	Muscovite	WBY3-21-3	Average
SiO ₂	37.43	36.74	35.18	36.73	34.27	45.83	44.45	46.09	45.46			
TiO ₂	0.19	0.13	0.11	0.21	0.37	0.08	0.04	0.08	0.06			
Al ₂ O ₃	12.57	12.84	13.65	12.45	13.77	33.61	31.78	32.90	32.76			
FeO	24.55	24.81	25.51	23.92	25.06	2.73	3.19	3.42	3.11			
MnO	0.32	0.30	0.41	0.32	0.36	0.11	0.00	0.04	0.05			
MgO	10.58	11.98	12.17	10.83	10.56	2.18	2.03	2.59	2.27			
CaO	0.00	0.00	0.00	0.00	0.00	0.07	0.66	0.04	0.26			
Na ₂ O	0.11	0.16	0.14	0.13	0.09	0.24	0.57	0.49	0.43			
K ₂ O	8.65	8.20	6.99	8.53	5.56	10.73	10.50	10.85	10.69			
Total	94.40	95.15	94.15	93.10	90.03	95.57	93.23	96.48	95.09			
Number of cation on the basis of 11 oxygen atoms												
Si	2.95	2.87	2.78	2.93	2.81	3.07	3.08	3.08	3.08			
Al ^{IV}	1.05	1.13	1.22	1.07	1.19	0.93	0.92	0.92	0.92			
Al ^{VI}	0.12	0.06	0.05	0.10	0.14	1.73	1.67	1.67	1.69			
Ti	0.01	0.01	0.01	0.01	0.02	0.00	0.00	0.00	0.00			
Fe ³⁺	0.10	0.05	0.06	0.09	0.20	0.15	0.18	0.19	0.18			
Fe ²⁺	1.52	1.57	1.63	1.51	1.52	0.00	0.00	0.00	0.00			
Mn	0.02	0.02	0.03	0.02	0.02	0.01	0.00	0.00	0.00			
Mg	1.24	1.40	1.44	1.29	1.29	0.22	0.21	0.26	0.23			
Ca	0.00	0.00	0.00	0.00	0.00	0.01	0.05	0.00	0.02			
Na	0.02	0.02	0.02	0.02	0.01	0.03	0.08	0.06	0.06			
K	0.87	0.82	0.71	0.87	0.58	0.92	0.93	0.92	0.92			
Total	7.90	7.95	7.94	7.91	7.80	7.07	7.12	7.12	7.10			
OH ⁻	2.00	2.00	2.00	2.00	2.00	2.00	2.00	2.00	2.00			
MF	0.43	0.46	0.46	0.44	0.43	0.58	0.53	0.57	0.56			
Al ^{VI} + Fe ³⁺ + Ti	0.23	0.12	0.12	0.20	0.37	1.89	1.86	1.86	1.87			
Fe ²⁺ + Mn	1.54	1.59	1.65	1.53	1.54	0.01	0.00	0.00	0.00			
Ti/(Mg + Fe + Ti + Mn)	0.00	0.00	0.00	0.00	0.01	0.01	0.00	0.01	0.01			
Al/(Al + Mg + Fe + Ti + Mn + Si)	0.17	0.17	0.18	0.17	0.18	0.43	0.42	0.42	0.43			

Table 6

Representative electron microprobe data of chlorites from the Weibao deposit.

Sample	WBY3-14	WBY3-14-1	WBY3-14-2	WBY3-14-3	WBY3-14-4	Chlorite I	WBY3-21	WBY3-21-1	WBY3-21-2	WBY3-21-3	WBY3-21-4	Chlorite II	WBY3-21-5
SiO ₂	28.80	30.01	25.52	26.89	26.56	26.46	26.37	26.24	26.05	26.28			
Al ₂ O ₃	14.09	13.24	17.10	15.40	15.92	18.18	17.85	18.05	18.61	17.89			
MgO	17.22	17.14	12.01	9.92	10.35	13.65	13.26	13.35	13.29	13.37			
FeO	26.97	26.43	29.04	33.57	32.34	29.04	28.71	28.63	28.95	28.12			
MnO	0.52	0.50	0.66	0.43	0.47	0.50	0.52	0.50	0.46	0.46			
TiO ₂	0.06	0.05	0.01	0.07	0.05	0.00	0.00	0.02	0.00	0.00			
Na ₂ O	0.03	0.06	0.09	0.04	0.04	0.06	0.02	0.02	0.01	0.04			
K ₂ O	0.45	0.47	0.12	0.05	0.06	0.03	0.00	0.04	0.00	0.00			
CaO	0.11	0.08	0.03	0.24	0.28	0.00	0.00	0.05	0.00	0.06			
Total	88.25	87.99	84.57	86.59	86.06	87.92	86.73	86.88	87.38	86.23			
Number of cation on the basis of 14 oxygen atoms													
Si	3.37	3.49	3.21	3.44	3.38	3.16	3.19	3.17	3.13	3.18			
Al	1.94	1.82	2.53	2.32	2.39	2.56	2.54	2.57	2.64	2.55			
Mg	3.00	2.97	2.25	1.89	1.96	2.43	2.39	2.40	2.38	2.41			
Fe	1.19	1.16	1.37	1.61	1.55	1.30	1.31	1.30	1.31	1.28			
Mn	0.05	0.05	0.07	0.05	0.05	0.05	0.05	0.05	0.05	0.05			
Ti	0.01	0.00	0.00	0.01	0.00	0.00	0.00	0.00	0.00	0.00			
Na	0.01	0.01	0.02	0.01	0.01	0.01	0.00	0.00	0.00	0.01			
K	0.07	0.07	0.02	0.01	0.01	0.00	0.00	0.01	0.00	0.00			
Ca	0.01	0.01	0.00	0.03	0.04	0.00	0.00	0.01	0.00	0.01			
Total	9.64	9.59	9.48	9.36	9.38	9.52	9.49	9.50	9.51	9.50			
Al ^{IV}	0.63	0.51	0.79	0.56	0.62	0.84	0.81	0.83	0.87	0.82			
Al ^{VI}	1.31	1.31	1.74	1.76	1.76	1.72	1.73	1.73	1.77	1.74			
Fe/(Fe + Mg)	0.28	0.28	0.38	0.46	0.44	0.35	0.35	0.35	0.35	0.35			
Na ₂ O + K ₂ O + CaO	0.59	0.61	0.25	0.33	0.37	0.09	0.02	0.10	0.01	0.10			

fluid inclusion studies (Fang et al., 2015), the precipitation temperature of galena and sphalerite in the banded skarn is below the closure temperature of mica, suggesting that the Ar-Ar age can represent the age of mineralization. In this study, we first reported syn-mineralization muscovite Ar/Ar plateau age of 226.6 ± 2.3 Ma, which suggests that the Weibao deposit were formed in the Late Triassic. This age is very similar to the Triassic granodiorite (227.6 ± 2.3 Ma) to the northwest of Weibao (Fig. 2a; Zhou et al., 2015). Actually, the Weibao mineralization age coincides with those

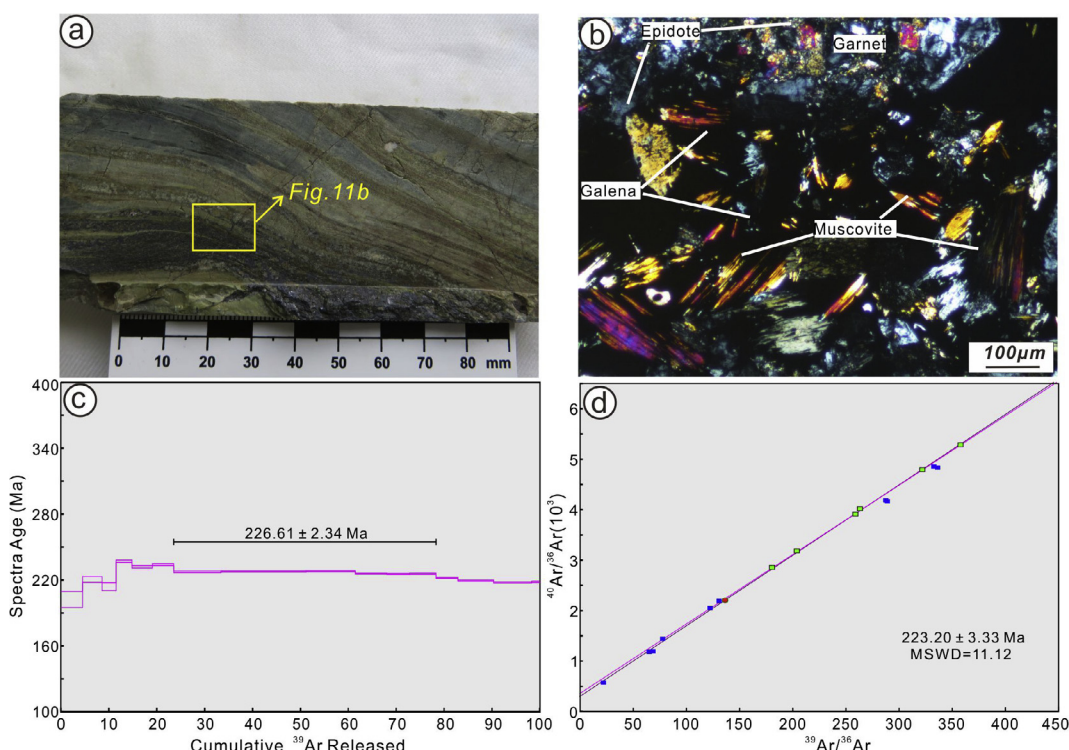
of some recently discovered skarn and porphyry-type deposits in the Qimantagh area, including the Binggounan Cu-Pb-Zn, Yazigou Cu-Mo, Hutouya Fe-Pb-Zn, Galinge Fe-Pb-Zn, Yemaquan Fe-Cu-Pb-Zn, Siyangjiao Pb-Zn, and Kendekeke Fe-Cu-Pb-Zn deposits (Fig. 1b; Feng et al., 2012; Gao et al., 2010; He et al., 2008; Zhao et al., 2013). A distinct characteristic of these deposits is that the mineralization is time-space closely related to the nearby Triassic granitoids (ca. 239–218 Ma), indicating an important magmatic-metallogenic event in the Qimantagh area (Feng et al., 2012; Zhao

Table 7

Representative electron microprobe data of sulfide minerals from the Weibao deposit.

Sample	WBY3-14		WBY3-24		WBY3-15		WBY3-14		WBY3-24		WBY3-15		WBY3-14		
	Mineral	Sp	Sp	Sp	Sp	Sp	Gn	Gn	Gn	Gn	Gn	Gn	Ccp	Ccp	
Se	0	0	0	0.01	0	0	0.01	0.02	0.02	0.05	0.04	0.01	0.03	0.01	0.01
As	0	0	0.02	0	0	0.01	0	0	0	0	0	0	0	0	0
Fe	4.61	5.37	3.68	3.84	5.95	6.88	0.06	0.11	0.06	0.07	0.07	0	0.01	28.57	29.08
Co	0.09	0.05	0.07	0.08	0.08	0.06	0	0	0	0	0	0	0.05	0.07	
Ni	0	0	0	0.01	0.01	0	0.01	0.01	0	0	0	0	0	0	
Cu	4.31	5.94	2.59	3.34	0.61	0.01	0.07	0.19	0	0	0.01	0	0	34.03	34.19
Zn	56.55	54	59.34	58.03	58.37	58.39	0.11	0.09	0.77	0.82	0.59	0.03	0	0	0
Ag	0.01	0	0	0	0	0.01	0	0	0	0	0	0	0	0.02	0.04
Cd	0	0.06	0.13	0.15	0	0	0	0.01	0	0	0	0	0	0	0
S	32.55	33.18	33.48	33.48	33.37	33.37	13.31	13.28	13.35	13.3	13.24	13.34	13.21	34.4	34.36
Pb	0.07	0.16	0.07	0.03	0.13	0.09	85.83	85.81	86.76	86.72	85.63	86.13	85.87	0.18	0.14
Total	98.18	98.76	99.38	98.98	98.51	98.8	99.4	99.52	100.96	100.97	99.57	99.5	99.13	97.27	97.88

Note: Sp-Sphalerite; Gn-Galena; Ccp-Chalcopyrite.

**Fig. 11.** (a) and (b) Photographs and photomicrograph showing the occurrence of muscovite; (c) and (d) $^{40}\text{Ar}/^{39}\text{Ar}$ plateau and corresponding isochron ages of muscovite.**Table 8** $^{39}\text{Ar}/^{40}\text{Ar}$ results by stepwise laser ablation dating for muscovite.

No.	Percent	^{36}Ar	^{37}Ar	^{38}Ar	^{39}Ar	^{40}Ar	Age (Ma)	$\pm 2\sigma$	^{40}Ar	^{39}Ar	K/Ca	$\pm 2\sigma$
15WHA0265B-001	4.0%	32.49379	851.121	4.1314256	719.030	8906.02	202.26	± 7.39	48.12	4.54	0.327	± 0.008
15WHA0265B-002	4.5%	9.86147	771.156	2.4298775	642.998	8727.13	220.50	± 2.63	74.96	4.06	0.323	± 0.007
15WHA0265B-003	5.0%	6.77642	744.253	3.1685907	465.133	6114.78	213.97	± 3.66	75.32	2.94	0.242	± 0.006
15WHA0265B-004	5.5%	0.00000	0.000	0.0000000	0.000	65.90	224.21	± 0.00	100.00	0.00	0.238	± 0.007
15WHA0265B-005	6.0%	6.74957	401.565	0.0000000	525.215	7698.35	237.02	± 1.13	79.41	3.32	0.506	± 0.010
15WHA0265D-001	6.5%	5.52193	725.856	0.0000000	675.876	9682.82	231.99	± 1.04	85.57	4.27	0.360	± 0.006
15WHA0265D-002	7.0%	5.38140	725.205	0.0000000	703.960	10175.82	233.95	± 0.88	86.47	4.44	0.376	± 0.007
15WHA0265D-003	8.0%	8.60086	3110.880	0.0000000	1561.802	21903.36	227.40	± 0.70	89.59	9.86	0.194	± 0.003
15WHA0265D-004	9.0%	13.77142	5220.449	0.0000000	2816.337	39574.19	227.82	± 0.55	90.66	17.78	0.209	± 0.003
15WHA0265D-005	10.0%	6.16827	2110.640	0.0000000	1625.896	22861.09	227.95	± 0.51	92.60	10.27	0.298	± 0.005
15WHA0265D-006	12.0%	3.23328	2059.020	0.0000000	1043.277	14517.25	225.73	± 0.47	93.81	6.59	0.196	± 0.003
15WHA0265F-001	14.0%	2.08206	1352.019	0.0000000	746.566	10377.63	225.51	± 0.51	94.39	4.71	0.214	± 0.004
15WHA0265F-002	17.0%	3.37676	1626.349	0.0000000	876.368	12192.22	225.69	± 0.59	92.42	5.53	0.209	± 0.003
15WHA0265F-003	20.0%	2.17844	1743.294	0.0000000	726.117	9917.81	221.82	± 0.52	93.89	4.58	0.161	± 0.003
15WHA0265F-004	25.0%	4.09163	3758.224	0.0000000	1178.119	15909.17	219.45	± 0.55	92.92	7.44	0.121	± 0.002
15WHA0265F-005	30.0%	4.33930	4361.592	0.0000000	1254.184	16792.76	217.70	± 0.51	92.89	7.92	0.111	± 0.002
15WHA0265F-006	40.0%	0.82446	798.709	0.0000000	277.853	3733.46	218.42	± 0.64	93.86	1.75	0.135	± 0.002

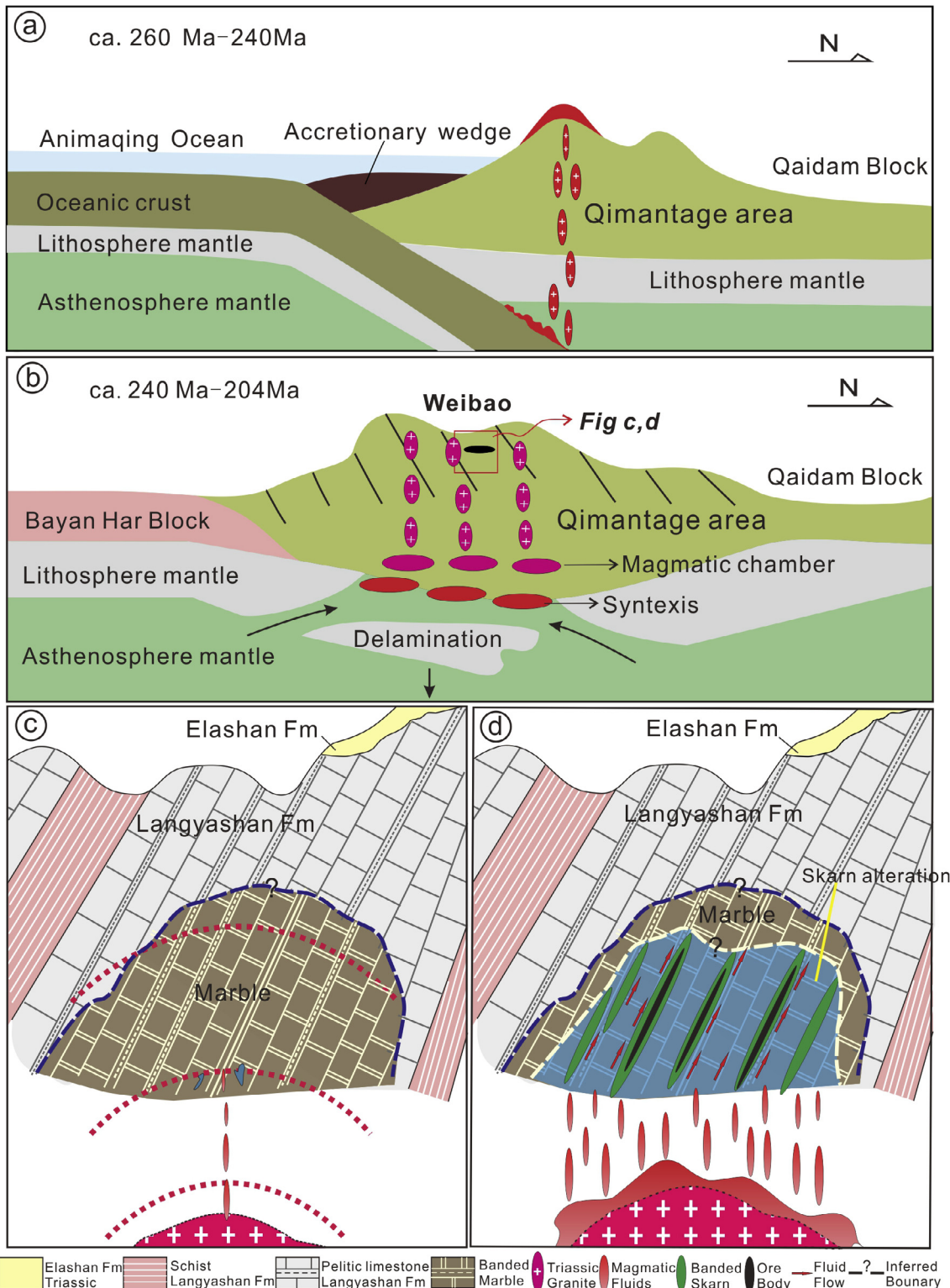


Fig. 12. Schematic metallogenetic model for the Weibao Pb-Zn deposit. (a) In the Permian (ca. 260 Ma), the Animaqing ocean basin may have begun to subduct northward beneath the Qaidam block and finally closed at ca. 240 Ma (b) In the Triassic (ca. 240–204 Ma), the Qimantagh area may have been in a post-collisional setting, with widespread emplacement of intermediate to felsic granitoids. (c) Emplacement of Triassic granitoids at depth may have induced isochemical metamorphism of pelitic limestone, turning it into banded marble. A small amount of magmatic fluids may have exsolved from the crystallizing magma (causing minor skarn alteration represented by Garnet I and Pyroxene I). (d) As the magma further fractionated, a large amount of magmatic fluids may have exsolved and reacted with the Langyashan Formation pelitic limestone, forming the banded skarn.

et al., 2013). Taking all the above-mentioned geological evidence into consideration, we propose that Weibao is also a magmatic-fluids-induced skarn deposit, which may have been genetically related to deep-lying Triassic granitoids (Fig. 12).

The Qimantagh area is situated in a Paleozoic subduction-related arc-trench zone, and has likely experienced multistage tectonic evolution from the Precambrian to the Jurassic. The basement of the Qimantagh area, represented by the Jinshukou Group, was

formed in the Paleoproterozoic (Lu et al., 2009). In the Early Paleozoic, the Qimantagh area may have been part of an arc-basin system in the Proto-Tethys, which subsequently evolved into an active continental margin at about the Early Paleozoic to the Early Mesozoic. In the Permian (~260 Ma), the Animaqing ocean began to subduct northward beneath the Qaidam block and finally closed at ca. 240 Ma (Fig. 12a), followed by the intercontinental collision (ca. 240–204 Ma) between the Bayan Har block and Eastern Kunlun orogen (Fig. 12b) (Feng et al., 2012; Guo et al., 1998; Li et al., 2008; Liu et al., 2004). At ca. 240–204 Ma, the Qimantagh area was in a post-orogenic extensional setting (Feng et al., 2012; Liu et al., 2004; Luo et al., 2002). This may have caused crustal thinning and the accompanied magma underplating, leading to material exchange and mixing between the mantle and the crust, as well as the regional extensive intermediate-felsic magmatism (Fig. 12b). Magmatic fluids derived from these intermediate-felsic intrusive rocks have likely contributed to many important Triassic mineralization events in the Qimantagh area, including that at Weibao.

8. Conclusion

1. The Weibao Pb-Zn skarn deposit is characterized by its banded appearance.
2. Mineral compositional and textural evidence suggests that the banded skarn was formed by infiltrative metasomatism of magmatic fluids, rather than by bimetasomatism between marble

Appendix A

Description of samples for analysis.

Sample No.	Sample Site	Depth (m)	Lithology	Mineralogy	Studying Method
WBY3-9	ZK007	159	Banded skarn	Zoned Grt II and Px II aggregates, Ep, Chl II, Cal + Qz + Ab veins	microscopic petrography; EPMA
WBY3-14	ZK007	196	Banded skarn	Zoned Grt II and Px II aggregates, Ep, Am II, Chl I, Sp, Gn, Py	microscopic petrography; EPMA
WBY3-15	ZK007	234	Banded skarn	Zoned Grt II and Px II aggregates, Ep, Am II, Bi, Gn, Qz	microscopic petrography; EPMA
WBY3-17	ZK007	257	Banded skarn	Zoned Grt II and Px II aggregates, Grt III + Sp + Gn + Cal veinlets	microscopic petrography; EPMA
WBY3-20	ZK007	314	Banded skarn	Zoned Grt II and Px II aggregates, Ep, disseminated Mgt, Qz, Cal veinlets, Ser	microscopic petrography; EPMA
WBY3-21	ZK007	327	Banded skarn	Zoned Grt II and Px II aggregates, Chl II + Qz + Cal, Mus, Sp, Gn, Ccp	microscopic petrography; EPMA; Ar-Ar dating
WBY3-24	ZK007	349	Banded skarn	Zoned Grt II and Px II aggregates, Ep, Am, Qz + Cal veins	microscopic petrography; EPMA
WBY3-25	ZK007	360	Banded skarn	Zoned Grt II and Px II aggregates, epitaxial Px II veins, Ep	microscopic petrography; EPMA
WBY3-31	ZK007	383	Banded marble	Recrystallized Cal, minor poikilitic Grt I and minor Ep	microscopic petrography; EPMA
WBY3-34	ZK007	397	Skarnized marble	Recrystallized Cal, poikilitic Grt I, Px I and Am I	microscopic petrography; EPMA

Appendix B

Composition of garnets (B1) and pyroxenes (B2) in skarn rocks formed by regional metamorphism.

Sample No.	SiO ₂	TiO ₂	Al ₂ O ₃	Cr ₂ O ₃	FeO ^T	MnO	MgO	CaO	Ref.
Appendix B1									
1	32.26	0.19	0.02	19.64	22.43	4.34	0.11	15.16	Pertoldova et al. (2009)
2	37.51	0.05	0.01	20.13	27.32	2.38	0.37	12.10	
3	36.93	0.11	0.01	20.29	22.34	9.79	0.42	8.77	
4	37.12	0.10	0.02	20.88	30.96	0.48	1.47	8.39	
5	37.20	0.22	0.00	14.64	12.06	0.14	0.08	28.80	
6	38.02	0.18	0.00	19.63	15.22	0.97	0.36	24.65	
7	38.02	0.09	0.01	18.79	16.96	1.77	0.22	24.09	
8	38.02	0.18	0.00	19.63	15.22	0.97	0.36	24.65	
9	38.30	0.58	0.00	17.13	9.02	1.36	0.34	33.20	
10	38.29	0.48	0.00	17.80	9.14	1.36	0.39	33.08	
11	37.20	0.28	0.02	19.22	9.13	0.70	0.03	31.78	
12	38.03	0.31	0.02	19.13	10.94	0.94	0.05	30.26	
13	36.26	0.07	0.00	8.83	21.15	1.60	0.04	30.01	
14	36.73	0.00	0.00	10.01	16.40	0.30	0.05	34.62	
15	37.50	0.35	0.03	15.37	18.12	0.87	0.25	26.82	
16	38.43	0.18	0.01	19.53	13.80	0.12	0.60	27.54	
17	36.74	0.51	8.01	0.00	19.83	1.79	0.00	33.91	
18	34.77	0.00	0.27	0.00	31.34	1.67	0.51	31.94	
19	36.74	0.51	8.01	0.00	19.83	1.79	0.00	33.91	Stanton, 1989
20	34.77	0.00	0.27	0.00	31.34	1.67	0.51	31.94	
21	35.96	0.32	4.31	0.00	24.14	1.67	0.08	32.72	

Appendix B2

Sample No.	SiO ₂	TiO ₂	Al ₂ O ₃	FeO ^T	MnO	MgO	CaO	Na ₂ O	K ₂ O	Ref.
1	50.77	0.00	0.38	22.51	0.20	5.43	20.53	0.68	0.00	Pertoldova et al. (2009)
2	53.85	0.11	6.63	10.70	0.03	7.92	17.06	4.48	0.00	
3	50.04	0.02	0.87	21.15	0.27	4.48	21.55	0.88	0.00	
4	51.48	0.11	4.88	16.04	0.13	5.70	16.99	4.00	0.00	
5	49.28	0.06	1.15	20.03	1.01	5.06	21.84	0.64	0.10	
6	50.65	0.11	0.84	18.75	0.32	6.68	23.62	0.09	0.00	
7	50.04	0.12	2.64	12.99	0.51	9.32	24.16	0.20	0.01	
8	52.23	0.08	1.25	12.31	1.15	10.59	23.00	0.22	0.01	
9	48.64	0.04	0.69	25.02	1.12	1.98	22.57	0.34	0.00	
10	51.72	0.00	0.67	13.37	0.22	9.23	23.55	0.49	0.00	
11	48.67	0.10	2.08	20.03	0.31	5.07	22.75	0.59	0.00	
12	47.79	0.14	2.19	21.76	0.36	3.83	22.27	0.61	0.00	
13	49.82	0.03	0.47	22.62	0.82	3.70	22.42	0.33	0.00	
14	54.49	0.00	0.37	1.10	0.19	17.54	25.74			Stanton, 1989
15	54.80	0.00	1.24	1.40	0.34	17.41	23.40			
16	54.51	0.00	0.62	1.21	0.27	17.30	25.81			

References

- Barnes, R.G., 1983. Stratiform and stratabound tungsten mineralization in the Broken Hill Block. *NSW. J. Geol. Soc. Aust.* 30, 225–239.
- Barnes, H.L., 1997. *Geochemistry of Hydrothermal Ore Deposits*. John Wiley and Sons, New York, pp. 303–358.
- Calagari, A.A., Hosseinzadeh, G., 2006. The mineralogy of copper-bearing skarn to the east of the Sungun-Chay river, East-Azerbaijan. *Iran. J. Asian Earth Sci.* 28, 423–438.
- Carmichael, I.S.E., 1966. The iron-titanium oxides of salic volcanic rocks and their associated ferromagnesian silicates. *Contrib. Mineral. Petrol.* 14, 36–64.
- Chang, Z.S., Meinert, L.D., 2008. The Empire Cu-Zn Mine, Idaho: exploration implications of unusual skarn features related to high fluorine activity. *Econ. Geol.* 103, 909–938.
- Chen, Y.J., Chen, H.Y., Zaw, K., Pirajno, F., Zhang, Z.J., 2007. Geodynamic settings and tectonic model of skarn gold deposits in China: an overview. *Ore Geol. Rev.* 31, 139–169.
- Ciobanu, C.L., Cook, N.J., 2004. Skarn textures and a case study: the Ocna de Fier-Dogenecea orefield, Banat, Romania. *Ore Geol. Rev.* 24, 315–370.
- Deer, W.A., Howie, R.A., Zussman, J., 1997. *Rock-Forming Minerals. 2B. Double-chain Silicates*. Geological Society, London, pp. 1–764.
- Dietvorst, E.J.L., 1982. Retrograde garnet zoning at low pressure in metapeleitic rocks from Kemio, SW Finland. *Contrib. Mineral. Petrol.* 79, 37–45.
- Fang, J., Chen, H., Zhang, L., Zheng, Y., Li, D., Wang, C., Shen, D., 2015. Ore genesis of the Weibao lead-zinc district, Eastern Kunlun Orogen, China: constraints from ore geology, fluid inclusion and isotope geochemistry. *Int. J. Earth Sci.* 104, 1209–1233.
- Feng, C.Y., Wang, S., Li, G.C., Ma, S.C., Li, D.S., 2012. Middle to Late Triassic granitoids in the Qimantage area, Qinghai Province, China: chronology, geochemistry and metallogenic significances. *Acta Petrol. Sin.* 28, 665–678 (in Chinese with English Abstract).
- Frantz, J.D., Mao, H., 1976. Bimetamorphism resulting from intergranular diffusion; I, A theoretical model for monomineralic reaction zone sequences. *Am. J. Sci.* 276, 817–840.
- Foster, M., 1960 Interpretation of the composition of lithium micas. U.S. Geological Survey Professional Paper 354-E, 115–147.
- Gao, Y.B., Li, W.Y., Tan, W.J., 2010. Metallogenetic characteristics and analysis of the prospecting potential in the area of Qimantage. *Northwest. Geol.* 4, 35–43 (in Chinese with English Abstract).
- Gao, Y.B., Li, W.Y., Qian, B., Li, K., Zhang, Z.W., Jiang, Z.X., Sheng, D.L., Wang, Z.H., Ye, M.F., 2014. Geology, fluid inclusions and S, Pb isotopic geochemistry of the Weibao Zn-Pb deposit in Qimantage, Xinjiang. *J. Jilin Univ. (Earth Sci. Edi.)*, 44, 1153–1165 (in Chinese with English Abstract).
- Gaspar, M., Knaack, C., Meinert, L.D., Moretti, R., 2008. REE in skarn systems: a LA-ICP-MS study of garnets from the Crown Jewel gold deposit. *Geochim. Cosmochim. Acta* 72, 185–205.
- Geophysical and Geochemical Party, Xinjiang Bureau of Geology and Mineral Resource (abv. GGP), 2010. Report for Geological Reconnaissance in the Weibao Lead-Zinc District in Ruqiang County, Xinjiang Uygur Autonomous Region. pp 1–201 (in Chinese).
- Guo, Z.F., Deng, J.F., Xu, Z.Q., Mo, X.X., Luo, Z.H., 1998. Late Paleozoic-Mesozoic intracontinental orogenic process and intermediate-acidic igneous rocks from the Eastern Kunlun mountains in north Tibet, northwestern China. *Geoscience* 12, 344–352 (in Chinese with English Abstract).
- Guy, B., 1993. Banded skarns, an example of geochemical dissipative structure. <<https://hal-sde.archives-ouvertes.fr/hal-00523251/>>.
- Harrison, T.M., Duncan, I., McDougall, I., 1985. Diffusion of ⁴⁰Ar in biotite: temperature, pressure and compositional effects. *Geochim. Cosmochim. Acta* 49, 2461–2468.
- He, S.Y., Qi, L.Y., Shu, S.L., Yin, H.Z., He, S.F., Jing, X.Y., 2008. Metallogenetic environment and potential in the Qimantage porphyry copper deposit, Qinghai. *Geol. Pros.* 2, 14–22 (in Chinese with English Abstract).
- Hu, H.W., Jing, B.S., Wang, S.L., Shu, L., 2010. Brief analysis for geological features and ore deposit origin of Weibao Lead-Zinc Deposit in Ruqiang County, Xinjiang. *Northwest. Geol.* 4, 73–80 (in Chinese with English abstract).
- Jamtveit, B., Wogelius, R.A., Fraser, D.G., 1993. Zonation patterns of skarn garnets: records of hydrothermal system evolution. *Geology* 21, 113–116.
- Jurek, K., Hulínský, V., 1980. The use and accuracy of the ZAF correction procedure for the microanalysis of glasses. *Microchim. Acta* 73, 183–198.
- Koppers, A.A., 2002. ArArCALC—software for ⁴⁰Ar/³⁹Ar age calculations. *Comput. Geosci.* 28, 605–619.
- Kwak, T.A., 2012. W-Sn Skarn Deposits: And Related Metamorphic Skarns and Granitoids. Elsevier, Amsterdam, pp. 1–400.
- Leake, B.E., Woolley, A.R., Birch, W.D., Burke, E.A., Ferraris, G., Grice, J.D., Stephenson, N.C., 2004. Nomenclature of amphiboles: additions and revisions to the International Mineralogical Association's amphibole nomenclature. *Mineral. Mag.* 68, 209–215.
- L'Heureux, I., 2013. Self-organized rhythmic patterns in geochemical systems. *Philos. Trans. R. Soc. London A* 371, 20120356.
- Li, R.S., Ji, W.H., Yang, Y.C., 2008. *The Geology of Kunlun Mountains and Its Adjacent Areas*. Geological Publishing House, Beijing, pp. 310–347 (in Chinese).
- Li, W., Neubauer, F., Liu, Y.J., Genser, J., Ren, S., Han, G.Q., Liang, C.Y., 2013. Paleozoic evolution of the Qimantagh magmatic arcs, Eastern Kunlun Mountains: constraints from zircon dating of granitoids and modern river sands. *J. Asian Earth Sci.* 77, 183–202.
- Liu, C.D., Mo, X.X., Luo, Z.H., Yu, X.H., Chen, H.W., Li, S.W., Zhao, X., 2004. Mixing events between the crust-and-mantle-derived magmas in Eastern Kunlun: evidence from zircon SHRIMP II chronology. *China Sci. Bull.* 49, 828–834 (in Chinese with English Abstract).
- Liu, X.J., Liu, W., Liu, L.J., 2012. The generation of a stratiform skarn and volcanic exhalative Pb-Zn deposit (Sawusi) in the southern Chinese Altay Mountains: the constraints from petrography, mineral assemblage and chemistry. *Gondwana Res.* 22, 597–614.
- Logan, M.A.V., 2000. Mineralogy and geochemistry of the Gualilan skarn deposit in the Precordillera of western Argentina. *Ore Geol. Rev.* 17, 113–138.
- Lu, H.Z., Liu, Y., Wang, C., Xu, Y., Li, H., 2003. Mineralization and fluid inclusion study of the Shizhuoyuan W-Sn-Bi-Mo-F skarn deposit, Hunan Province, China. *Econ. Geol.* 98, 955–974.
- Lu, S.N., Li, H.K., Wang, H.C., Chen, Z.H., Zheng, J.K., Xiang, Z.Q., 2009. Detrital zircon population of Proterozoic meta-sedimentary strata in the Qinling-Qilian-Kunlun Orogen. *Acta Petrol. Sin.* 25, 2195–2208 (in Chinese with English abstract).
- Luo, Z.H., Ke, S., Cao, Y.Q., Deng, J.F., Zhan, H.W., 2002. Late Indosinian mantle-derived magmatism in the East Kunlun. *Geol. Bull. China* 21, 292–297 (in Chinese with English Abstract).
- Meinert, L., Hedenquist, J., Satoh, H., Matsuhisa, Y., 2003. Formation of anhydrous and hydrous skarn in Cu-Au ore deposits by magmatic fluids. *Econ. Geol.* 98, 147–156.
- Meinert, L., Dipple, G., Niculescu, S., 2005. World skarn deposits. *Econ. Geol.* 100, 299–336.
- Moecher, D.P., Chou, I.M., 1990. Experimental investigation of andradite and hedenbergite equilibria employing the hydrogen sensor technique, with revised estimates of $\Delta_f G_{m,298}^0$ for andradite and hedenbergite. *Am. Mineral.* 75, 1327–1341.
- Newberry, R., Dillon, J., Adams, D., 1986. Regionally metamorphosed, calc-silicate-hosted deposits of the Brooks Range, northern Alaska. *Econ. Geol.* 81, 1728–1752.
- Oen, I., de Maesschalck, A., Lustenhouwer, W., 1986. Mid-Proterozoic exhalative-sedimentary Mn skarns containing possible microbial fossils, Grythyttan, Bergslagen, Sweden. *Econ. Geol.* 81, 1533–1543.
- Ortleva, P., Chadam, J., Merino, E., Sen, A., 1987. Geochemical self-organization II: the reactive-infiltration instability. *Am. J. Sci.* 287, 1008–1040.
- Palinkaš, S.S., Palinkaš, L.A., Renac, C., Spangenberg, J.E., Lüders, V., Molnar, F., Maliqi, G., 2013. Metallogenetic model of the Trepcă Pb-Zn-Ag Skarn Deposit,

- Kosovo: evidence from fluid inclusions, rare earth elements, and stable isotope data. *Econ. Geol.* 108, 135–162.
- Peng, H.J., Zhang, C.Q., Mao, J.W., Santosh, M., Zhou, Y.M., Hou, L., 2015. Garnets in porphyry-skarn systems: A LA-ICP-MS, fluid inclusion, and stable isotope study of garnets from the Hongniu-Hongshan copper deposit, Zhongdian area, NW Yunnan Province, China. *J. Asian Earth Sci.* 103, 229–251.
- Pertoldova, J., Tycova, P., Verner, K., Kosulicova, M., Pertold, Z., Kosler, J., Konopasek, J., Pudilova, M., 2009. Metamorphic history of skarns, origin of their protolith and implications for genetic interpretation; an example from three units of the Bohemian Massif. *J. Geosci.* 54, 101–134.
- Qiu, H.N., Wijbrans, J.R., 2008. The Paleozoic metamorphic history of the Central Orogenic Belt of China from $^{40}\text{Ar}/^{39}\text{Ar}$ geochronology of eclogite garnet fluid inclusions. *Earth Planet. Sci. Lett.* 268, 501–514.
- Robb, L., 2009. Introduction to Ore-Forming Processes. John Wiley and Sons, New York, pp. 129–214.
- Rusinov, V., Zhukov, V., 2008. Model for the development of rhythmically banded wollastonite-hedenbergite skarns at the Dal'negorsk deposit, southern Russian Far East. *Geochim. Int.* 46, 789–799.
- Stanton, R., 1989. The precursor principle and the possible significance of stratiform ores and related chemical sediments in the elucidation of processes of regional metamorphic mineral formation. *Philos. Trans. R. Soc. London A* 328, 529–646.
- Thompson, A.B., 1975. Calc-silicate diffusion zones between marble and pelitic schist. *J. Petrol.* 16, 314–346.
- Wan, B., Xiao, W., Zhang, L., Han, C., 2012. Iron mineralization associated with a major strike-slip shear zone: radiometric and oxygen isotope evidence from the Mengku deposit, NW China. *Ore Geol. Rev.* 44, 136–147.
- Wones, D.R., Eugster, H.P., 1965. Stability of biotite-experiment theory and application. *Am. Mineral.* 50, 1228–1272.
- Yang, Z.A., Peng, S.L., Shi, F.F., Zhu, G.C., Zou, L., 2008. Geological characteristics and genesis of the Weibao Pb-Zn deposit in Ruoqiang County, Xinjiang. *Mineral. Res. Geol.* 22, 503–505 (in Chinese with English abstract).
- Zhao, Y.M., Feng, C.Y., Li, D.X., Liu, J.N., Xiao, Y., Yu, M., Ma, S.C., 2013. Metallogenesis setting and mineralization-alteration characteristics of major skarn Fe-polymetallic deposits in Qimantag area, western Qinghai Province. *Miner. Deposition* 32, 1–19 (in Chinese with English Abstract).
- Zhou, J.H., Feng, C.Y., Shen, D.L., Li, D.X., Wang, H., Zhang, M.Y., Ma, S.C., 2015. Geochronology, Geochemistry and Tectonic Implications of Granodiorite in the Northwest of Weibao Deposit, Xinjiang Qimantage. *Acta Geol. Sin.* 89, 473–486 (in Chinese with English Abstract).